[24] Lanzilli G, Fuggetta MP, Tricarico, M, Cottarelli A, Serafino A, Falchetti R, *et al.* Resveratrol down-regulates the growth and telomerase activity of breast cancer cells *in vitro*. Int J Oncol 2006; 28: 641-8.

[25] Gatz SA, Keimling M, Baumann C, Dork T, Debatin K-M, Fulda S, *et al.* Resveratrol modulates DNA double-strand break repair pathways in an ATM/ATR –p53 and –Nbs1 –dependent manner. Carcinogenesis 2008; 29: 519-27.

[26] Lagouge M, Argmann C, Gerhart-Hines Z, Meziane H, Lerin C, Daussin F, *et al.* Resveratrol improves mitochondrial function and protects against metabolic disease by activating SIRT1 and PGC-1α. Cell 2006; 127: 1109-22.

[27] van der Horst A and Burgering BMT. Stressing the role of FoxO proteins in lifespan and disease. Nat Rev Mol Cell Biol 2007; 8: 440-50.

[28] Manna SK, Mukhopadhyay A and Aggarwal BB. Resveratrol suppresses TNF-induced activation of nuclear transcription factors NF-κB, activator protein-1, and apoptosis: potential role of reactive oxygen intermediates and lipid peroxidation. J Immunol Meth 2000; 164: 6509-19.

Received: January 14, 2010 Revised: April 30, 2010 Accepted: November 2, 2010

2011年，第52回日本心身医学会総会ならびに学術講演会（横浜）

Jpn J Psychosom Med
52:194-200, 2012

シンポジウム：摂食障害の新たな展開

脂質代謝の変化からみたカロリー制限による抗老化・寿命延長作用のメカニズム

樋上賀一*

抄録：カロリー制限（caloric restriction：CR）は，老化過程を抑制，加齢に伴う疾患の発生を遅延し，平均および最大寿命を延長する唯一の簡便な再現性の高い方法として，老化研究に広く応用されている．しかし，そのメカニズムはいまだ解明されていない．一般にCRは，成長を抑制し，身体を小さく保ち，脂肪組織量を減少させ，高血糖および高インスリン血症を抑制，炎症を抑制，低体温で，脂質やエネルギー代謝を修飾し，内因性および外因性ストレスに対する抵抗性を増強，ミトコンドリア・バイオジェネーシスを亢進，サーチュインを活性化することが知られている．われわれは，CR動物では，食餌不足に対する適応反応として脂肪組織のリモデリングを介して脂質を効率的に利用していること，このような代謝の変化に脂肪酸合成関連遺伝子群発現の主要転写因子であるsterol regulatory element binding protein 1c（SREBP1c）が重要である可能性を示した．SREBP1cを介した*de novo*脂肪酸合成系の活性化がCRの主要なメカニズムの1つと考えられる．

Key words：カロリー制限，老化，脂質代謝，脂肪組織リモデリング，SREBP1c

カロリー制限の抗老化・寿命延長効果とは

1935年，米国のMcCayらは，離乳直後からの摂取カロリーの制限（caloric restriction：CR）により，ラットの寿命が延長することを報告した．それ以来75年以上にわたり，CRは，食餌制限（dietary restriction，food restriction），エネルギー制限（energy restriction）とも呼ばれ，唯一で簡便な再現性の高い寿命延長法として広く老化研究に応用されてきた[1)2)]．CRによる寿命延長効果は，酵母や線虫といった下等生物からげっ歯類にいたるまで広く観察されることから，進化の過程で保存されたメカニズムが関与することが示唆される．1989年Holliday[3)]は，CRによる抗老化・寿命延長作用のメカニズムとして，以下のように適応反応仮説を提唱し，食餌不足に対する神経内分泌および代謝の変化の重要性を進化論的観点から説明した．食餌が豊富な時期には，個体は成長し，強い大きな個体で積極的に生殖することで子孫を増やし，さらに過剰なエネルギーを脂肪組織に貯蔵する．一方，食餌が不足する時期には，個体の成長や生殖を抑制し，脂肪組織に貯えたエネルギーを使いながら，寿命を延長し，食餌が十分に得られる時期を待つ．このような食餌不足に対する適応能力の発達した動物が，進化の過程で選択されてきた．CRは，この食餌不足に対する適応反応を活性化し，抗老化・寿命延長をもたらすのではないかと考えられる．

*東京理科大学薬学部生命創薬科学科分子病理・代謝学研究室（連絡先：樋上賀一，〒278-8510 千葉県野田市山崎2641）

ほ乳類では，げっ歯類を中心に研究され，CRはさまざまな生理的加齢現象を抑制，老化に伴って発症する種々の疾患発症を遅延もしくは抑制し，寿命を延長することが明らかとなってきた．CRは活動性を維持し，平均および最大寿命を延長すること，CRの効果は，その期間や程度に比例すること，またエネルギー摂取の抑制にのみ依存しており，エネルギー制限のない各栄養素の摂取制限（糖質，脂質制限，タンパク質の摂取制限など）では，効果は得られないことが報告されている[1)2)]．一般的に，CR動物では，高血糖や高インスリン血症の抑制，酸化ストレスを含む内因性ストレスおよび外因性環境ストレスに対する抵抗性の増強，炎症の抑制，低体温，エネルギー代謝の効率化，ミトコンドリア・バイオジェネシスの活性化，サーチュインの活性化などが観察されており，これらがCRによる抗老化・寿命延長効果に重要であろうと考えられている．しかしながら，その詳細なメカニズムはいまだ解明されていない[4)〜6)]．

米国では1980年代の後半から数施設において，霊長類においてもCRの効果が有効であるか，サルを用いて検証されている．サルの寿命が長いことから最終的な結論は出ていないが，げっ歯類で観察されるCR動物の表現型はサルにおいても観察されることなどから，CRは霊長類においても有用であろうと考えられている[7)8)]．また，CRされたサルで観察された低体温，低血糖および年齢に伴って低下するdehydroepiandrosterone（DHEAS）の減少率が低いヒトの集団は，そうでない集団に比べて平均余命が長いことも報告されている[9)]．それゆえ，CRの有益な効果は，げっ歯類のみならず，ヒトを含む霊長類においても有効であろうと考えられる．

単一遺伝子の変異により長寿命を示すマウスやラット

CR以外寿命を延長する方法がなかったが，米国のBartkeら[10)]は1996年，Ames矮小マウスが長寿を示すと報告した．Ames矮小マウスは下垂体の発生や分化にかかわる転写因子であるProp1遺伝子に変異があり，成長ホルモンなどの下垂体前葉ホルモンの分泌に障害がある．Prop1遺伝子と類似した機能を有するPit1遺伝子に変異のあるSnell矮小マウス，次いで成長ホルモン放出ホルモン受容体遺伝子に変異のあるLittleマウスが長寿であることも報告された．その後，分子生物学および分子遺伝学の進歩と相まって，成長ホルモン受容体遺伝子やインスリン様成長因子1受容体遺伝子をノックアウトしたマウスなどが次々に作られ，筆者の知る限り現在まで報告されている単一遺伝子の改変により長寿を示すマウスやラットは約20種以上に及ぶ[11)]．これらを分類すると，その半数は成長ホルモン（GH）/インスリン様成長因子1（IGF-1）シグナルに関連する遺伝子を修飾したものであり，酸化ストレス/レドックス制御に関連するもの，脂肪細胞もしくはアディポサイトカインに関連するもの，およびその他の4つに大別できる．

われわれも，アンチセンス成長ホルモン遺伝子を成長ホルモン産生細胞に発現するようなトランスジェニック（tg）ラットにおいて，寿命を検討した．するとホモラット（tg/tg）の寿命はかえって短縮したが，ヘテロ（tg/−）ラットでは平均および最大寿命とも5〜10%延長した[12)]．CRにおいてもGH/IGF-1シグナルは抑制されるため，CRの有益な作用はGH/IGF-1シグナルの抑制に関連すると示唆された．そこで，野生型ラットと寿命が延長した（tg/−）ラットにCRを行った．すると予想に反して，野生型および（tg/−）ラットとも平均および最大寿命が同程度延長した[13)]．このことは，GH/IGF-1シグナルの抑制はCRの主要なメカニズムでないことを示唆している．

Table 1　CR と GH/IGF-1 抑制との比較

	CR による変化		GH/IGF-1 抑制による変化
	摂食後	摂食前	
血液生化学データ			
総脂質	↓	↓	↓
トリグリセリド	↓	↓	↓
総コレステロール	↓	↓	→
遊離コレステロール	↓	↓	↓
リン脂質	↓	↓	↓
遊離脂肪酸	↓	→	→
ケトン体	→	↑	→
グルコース負荷試験	↑		↑
インスリン負荷試験	↑		↑
肝臓の遺伝子発現			
β酸化関連遺伝子	→	↑	→
脂肪酸合成関連遺伝子	↑	↓	→
ストレス応答遺伝子	→	↑	↑
白色脂肪組織の遺伝子発現			
脂肪酸合成関連遺伝子	↑		→
炎症関連遺伝子	↓		→

成長ホルモン（GH）/インスリン様成長因子 1（IGF-1）シグナル非依存的な CR のメカニズム

われわれは，同程度に寿命が延長した野生型（−/−）CR ラット（以下，CR ラット）および（tg/−）自由摂食ラット（以下，Tg ラット）のさまざまなパラメーターを野生型（−/−）自由摂食ラット（以下，AL ラット）と比較することで，GH/IGF-1 シグナル非依存的な CR の影響を明らかにしようと試みた．

血清総脂質，トリグリセリド，遊離コレステロール，リン脂質レベルは，AL ラットに比較して，摂食状態にかかわらず CR ラットおよび Tg ラットで，同様に有意に低値を示した．一方，CR による摂食後の遊離脂肪酸の低下および摂食後のケトン体の増加は，Tg ラットでは観察できなかった[14]．また，グルコース負荷試験およびインスリン負荷試験では，CR ラットでも Tg ラットでも，グルコース耐性およびインスリン高感受性を示した[15]．肝臓の網羅的遺伝子発現解析では，CR により摂食前ではミトコンドリアβ酸化関連遺伝子の発現が亢進した．また摂食後では脂肪酸合成関連遺伝子の発現が顕著に亢進した．しかしながら，これら遺伝子発現の変化は Tg ラット肝臓では観察できなかった．一方，MDR2 や OCT1A などストレス耐性遺伝子発現の亢進は CR ラットでも Tg ラットでも，同様に観察された（**Table 1**）．以上の結果から，CR により摂食前にはミトコンドリアβ酸化を介して脂質をエネルギー源とし，摂食後には脂質を貯蔵するシステムが活性化していること，この CR による代謝の変化は GH/IGF-1 非依存性に制御されていることが示唆された[14]．

前述したように，単一遺伝子の改変により長寿を示すと報告されているマウスやラットに，脂肪細胞特異的にもしくはアディポサイトカイン分泌を修飾したマウスが含まれる．具体的には脂肪特異的にインスリン受容体をノックアウトしたマウス，脂肪細胞の分化因子である c/EBPβ を c/EBPα locus にノックインした c/EBPβ/β マウス，さらに脂肪細胞特異的なサイトカインでありインスリン感受性を正に制御し，抗炎症性サイトカインでもあるアディポネクチンを肝臓で過剰発現させたトランスジェニックマウスが長寿命であることが報告されて

Table 2　SREBP1c による影響およびカロリー制限における SREBP1c の影響

	SREBP1cKO による影響	CR による影響			
		野生型マウス		SREBP1cKO マウス	
		摂食後	摂食前	摂食後	摂食前
寿命	↓	↑		→	
呼吸商	↑	↓		↓	
グルコース負荷試験	→	↑		→	
インスリン負荷試験	→	↑		→	
腹部内臓脂肪組織量	↓	↓↓		↓	
肩甲骨間褐色脂肪組織量	→	↓		→	
血液生化学					
トリグリセリド	→	→	↓	→	→
遊離脂肪酸	→	↓	↓	→	→
ケトン体	↓	un	↓	un	→
肝臓含有脂質					
トリグリセリド	→	→	↓	→	↓
遊離脂肪酸	↑	→	→	→	→
心臓含有脂質					
トリグリセリド	→	→	→	→	→
遊離脂肪酸	→	→	↑	→	→

un：undetectable

いる[16)~18)]．すなわち，脂肪細胞の代謝や分化，アディポカインは寿命制御に重要であることが示唆される．

一方，CR による個体のサイズや体重の減少は，脂肪組織量の減少を伴う．CR は体重に比べ脂肪組織量，さらには内臓脂肪量により強い影響を与えるといわれている[19)]．われわれは，CR 群および対照群の精巣上体周囲白色脂肪組織での網羅的遺伝子発現解析を行い，CR が多くの糖，アミノ酸，脂質およびミトコンドリアエネルギー代謝関連遺伝子の発現を増強すること，一方，多くの炎症，血管新生，細胞外器質および細胞骨格関連遺伝子の発現を抑制することを明らかにした[20)21)]．このような遺伝子発現の変化は，摂食パターンに影響を受けなかった．また，遺伝子発現の変化の一部は，*in vitro* での脂肪細胞の分化に伴う遺伝子発現の変化と同様であり，一方，すでに報告されている肥満動物の脂肪組織での遺伝子発現とは，逆相関する傾向を示した[20)21)]．さらに，CR ラットおよび Tg ラット，AL ラットの精巣上体周囲脂肪組織において，形態学的および網羅的遺伝子発現解析を行った．その結果，AL ラットに比較して，CR ラットの脂肪細胞のサイズは顕著に小型化したが，Tg ラットでの変化は乏しかった．また，CR ラットでは脂肪酸合成関連遺伝子の発現が亢進し，炎症関連遺伝子の発現は抑制されたが，このような遺伝子発現の変化は Tg ラットでは観察されなかった（**Table 1**）．さらに，CR ラットでのみ発現が亢進した脂肪酸合成関連遺伝子の多くは脂肪酸合成系のマスター転写調節因子である sterol regulatory element binding protein (SREBP) 1 により制御される遺伝子群であった（未発表データ）．

以上より，血中の遊離脂肪酸およびケトン体レベルの変化，肝臓におけるミトコンドリアβ酸化と脂肪酸合成関連遺伝子発現の変化，脂肪組織における *de novo* 脂肪酸合成と炎症関連遺伝子の発現の変化，すなわち脂質代謝の変化と脂肪組織のリモデリングが，GH/IGF-1 シグナル非依存的な CR による変化と考えられ，その一部は SREBP1 により制御されている可能性が示唆された．

適応反応仮説からみたCRによる代謝の変化におけるSREBP1cの関与

さまざまなパラメーターにおいて，CRは絶食状態（fasting, starvation）とは異なるが，血中レプチン，インスリン，成長ホルモンおよびLHレベルはともに低値を示し，コルチコステロンレベルは高値を示すという変化は共通している[22)23)]．また絶食状態では，呼吸商（respiratory quotient）は低値を示し，エネルギー源が糖質から脂質へシフトし[24)25)]，白色脂肪組織由来の脂肪酸が，ミトコンドリアβ酸化の燃料として使われ，主に脳における燃料源であるケトン体が作られる[25)]．CRラットの呼吸商は，食餌摂取後では高値，摂取前では低値を示し，その日内変動は食餌摂取に依存し大きく変動する．一方，ALラットの呼吸商の日内変動は，CRラットに比べて小さい[26)]．そこで，われわれはSREBP1cノックアウト（KO）マウスと野生型マウスにおのおのCRを行い，寿命をはじめとするさまざまなパラメーターの解析を行った．その結果を**Table 2**に示す．SREBP1cKOマウス（以下，KOマウス）では，野生型マウスに比べて，平均および最大寿命とも有意に減少した．野生型マウスではCRに伴い平均および最大寿命とも延長したが，興味深いことにKOマウスではこのCRに伴う寿命延長効果がみられなかった．KOマウスでは野生型に比べて呼吸商は有意に高値を示し，日内変動も乏しかった．しかしながら，CR時の呼吸商は野生型，KOマウスとも有意な差はみられなかった．グルコース負荷試験およびインスリン負荷試験において，野生型ではCRによりグルコース耐性，インスリン感受性が亢進したが，KOマウスではこのようなCRの効果は失われていた．腹部内臓脂肪はKOマウスにおいて減少していた．CRにより野生型では腹部内臓脂肪量は顕著に減少したものの，KOマウスではその減少が乏しかった．また，肩甲骨間褐色脂肪組織量はCRにより野生型マウスでは顕著に減少するものの，KOマウスではこの減少がみられなかった．血液や肝臓および心臓含有トリグリセリドや遊離脂肪酸においても，野生型において観察されたCRの影響がKOマウスでは観察できないものがあった．摂食前の空腹時ケトン体レベルは野生型マウスに比べてKOマウスで減少した．野生型マウスではCRの空腹時ケトン体レベルは有意に増加したが，KOマウスではこのような変化は観察できなかった．以上の知見から，KOマウスではCRにより脂質をエネルギー源として有効に利用する能力が低下しているのではないかと考えられた（未発表データ）．

そこで，野生型およびKOマウスでの絶食に対する応答を比較した．するとKOマウスでは野生型に比べて，絶食に伴って観察される体重の減少，脂肪組織重量の減少，血糖値の低下および血清ケトン体の増加が抑制されていることが明らかとなった（未発表データ）．このことは，SREBP1cが絶食応答，さらにCRによる抗老化・寿命延長効果に重要な役割を担っていることを示唆する．

de novo 脂肪酸合成の重要性

われわれはCRおよび自由摂食ラットの白色脂肪組織においてプロテオーム解析を行った．その結果，CRによりATP-citrate lyase, NADP-dependent malic enzyme, pyruvate dehydrogenase E1 component subunit beta, pyruvate carboxylaseの発現が増加していた．さらに，citrate synthase活性が亢進していた．このことは，CRによりピルビン酸/リンゴ酸回路が活性化している可能性を示唆する（未発表データ）．また，前述したようにCRによりSREBP1cを介した脂肪酸合成が亢進していた．この2つのCR動物の白色脂肪組織の特徴を考え合わせると，白色脂肪組織はCR時エネルギー貯蔵装置としてではなく，グルコースをよりエネルギー効率の高い脂肪酸に変換する装置として機能している可

能性を示唆する．一方，がん悪液質の白色脂肪組織では，CR と同じように摂食量が減少した状態にもかかわらず，SREBP1c を介した脂肪酸合成は抑制されているようである[27]．この違いは，白色脂肪組織での *de novo* 脂肪酸合成が亢進されるか抑制されるかが，生理的なやせか病的なやせかの違いの１つになる可能性を示唆する．

おわりに

CR に関する研究は，主として老化生物学を専門とする研究者により研究されてきており，現在，この分野での CR に関する研究は，“その作用メカニズムの解明”に加え，“ヒトにおける CR の有効性”という２つの主要テーマに集約されている．そのうち前者に関して，白色脂肪組織リモデリングと SREBP1c を介した脂質代謝活性化の重要性を述べた．一方，同じく摂食量が減少した病態として，がん悪液質や神経性食欲不振症などの摂食障害があり，近年，モデル動物を用いた研究が広く行われるようになってきた．一般にがん悪液質における脂肪組織の萎縮は lipolysis の亢進によると考えられており，脂肪酸合成に関する知見は乏しい[27]．今まで異なった分野で研究されてきた CR モデルおよび摂食障害モデルから得られる知見を比較，検討することで，両分野に新たな切り口での研究の進展が期待される．

謝辞：第 52 回日本心身医学会総会のシンポジウムにおける講演の機会，さらにこの総説を執筆する機会を与えてくださった乾　明夫先生ならびに須藤信行先生に感謝いたします．

文献

1) Yu BP：Modulation of Aging Processes by Dietary Restriction. CRC Press, Boca Raton, 1994
2) Weindruch R, Walford RL：The Retardation of Aging and Disease by Dietary Restriction. Charles C Thomas, Springfield, 1988
3) Holliday R：Food reproduction and longevity：Is the extended lifespan of calorie-restricted animals an evolutionary adaptation? *Bioessays* **10**：125-127, 1989
4) Higami Y, Yamaza H, Shimokawa I：Laboratory findings of caloric restriction in rodents and primates. *Adv Clin Chem* **39**：211-237, 2005
5) Masoro EJ：Overview of caloric restriction and ageing. *Mech Ageing Dev* **126**：913-922, 2005
6) Sinclair DA：Toward a unified theory of caloric restriction and longevity regulation. *Mech Ageing Dev* **126**：987-1002, 2005
7) Colman RJ, Anderson RM, Johnson SC, et al：Caloric restriction delays disease onset and mortality in rhesus monkeys. *Science* **325**：201-204, 2009
8) Kemnitz JW：Calorie restriction and aging in nonhuman primates. *ILAR J* **52**：66-77, 2011
9) Roth GS, Lane MA, Ingram DK, et al：Biomarkers of caloric restriction may predict longevity in humans. *Science* **297**：811, 2002
10) Brown-Borg HM, Borg KE, Meliska CJ, et al：Dwarf mice and the ageing process. *Nature* **384**：33, 1996
11) Shimokawa I, Chiba T, Yamaza H, et al：Longevity genes：insights from calorie restriction and genetic longevity models. *Mol Cells* **26**：427-435, 2008
12) Shimokawa I, Higami Y, Utsuyama M, et al：Life span extension by reduction in growth hormone-insulin-like growth factor-1 axis in a transgenic rat model. *Am J Pathol* **160**：2259-2265, 2002
13) Shimokawa I, Higami Y, Tsuchiya T, et al：Life span extension by reduction of the growth hormone-insulin-like growth factor-1 axis：relation to caloric restriction. *FASEB J* **17**：1108-1109, 2003
14) Higami Y, Tsuchiya T, Chiba T, et al：Hepatic gene expression profile of lipid metabolism in rats：Impact of caloric restriction and growth hormone/insulin-like growth factor-1 suppression. *J Gerontol A Biol Sci Med Sci* **61**：1099-1110, 2006
15) Yamaza H, Komatsu T, Chiba T, et al：A transgenic dwarf rat model as a tool for the study of calorie restriction and aging. *Exp Gerontol* **39**：269-272, 2004
16) Blüher M, Kahn BB, Kahn CR：Extended longevity in mice lacking the insulin receptor in adipose tissue. *Science* **299**：572-574, 2003
17) Chiu CH, Lin WD, Huang SY, et al：Effect of a C/EBP gene replacement on mitochondrial biogenesis in fat cells. *Genes Dev* **18**：1970-1975, 2004
18) Otabe S, Yuan X, Fukutani T, et al：Overexpression of human adiponectin in transgenic mice results in suppression of fat accumulation and

prevention of premature death by high-calorie diet. *Am J Physiol Endocrinol Metab* **293**: E210-218, 2007
19) Barzilai N, Banerjee S, Hawkins M, et al: Caloric restriction reverses hepatic insulin resistance in aging rats by decreasing visceral fat. *J Clin Invest* **101**: 1353-1361, 1998
20) Higami Y, Pugh TD, Page GP, et al: Adipose tissue energy metabolism: altered gene expression profile of mice subjected to long-term caloric restriction. *FASEB J* **18**: 415-417, 2004
21) Higami Y, Barger JL, Page GP, et al: Energy restriction lowers the expression of genes linked to inflammation, the cytoskeleton, the extracellular matrix, and angiogenesis in mouse adipose tissue. *J Nutr* **136**: 343-352, 2006
22) Nelson JF: Neuroendocrine involvement in the retardation of aging by dietary restriction: A hypothesis. In: Yu BP (ed): Modulation of Aging Processes by Dietary Restriction. Boca CRC Press, Raton, Florida, pp37-55, 1994
23) Ahima RS, Prabakaran D, Mantzoros C, et al: Role of leptin in the neuroendocrine response to fasting. *Nature* **382**: 250-252, 1996
24) Overton JM, Williams TD, Chambers JB, et al: Central leptin infusion attenuates the cardiovascular and metabolic effects of fasting in rats. *Hypertension* **37**: 663-669, 2001
25) Salway JG: Metabolism at a Glance. Blackwell Science, Oxford, UK, 1999
26) McCarter RJ, Palmer J: Energy metabolism and aging: a lifelong study of Fischer 344 rats. *Am J Physiol* **263**: E448-452, 1992
27) Bing C, Trayhurn P: New insights into adipose tissue atrophy in cancer cachexia. *Proc Nutr Soc* **68**: 385-392, 2009

Abstract

Altered Energy Metabolism in Anti-aging and Pro-longevity Effects of Caloric Restriction

Yoshikazu Higami*

*Molecular Pathology & Metabolic Disease, Faculty of Pharmaceutical Sciences, Tokyo University of Science
(*Mailing Address*: Yoshikazu Higami, 2641 Yamazaki, Noda-shi, Chiba 278-8510, Japan)

Caloric restriction (CR) has been applied as a powerful tool in aging research. CR is accepted as a robust, reproducible and simple experimental manipulation known to extend both median and maximum lifespans, and to retard and suppress a broad spectrum of pathophysiological changes in a variety of mammals. In general, CR delays skeletal and sexual maturation, reduces body size with less adiposity, lowers body temperature, modulates hyperglycemia and insulinemia, alters lipid and energy metabolisms, protects against internal oxidative and environmental stresses, and activates mitochondrial biogenesis and sirtuins. Based on the adaptive response hypothesis against food shortage, I propose that CR promotes adipose tissue remodeling and modulates energy metabolism via sterol regulatory element binding protein (SREBP) 1c, a master transcriptional factor of fatty acid biosynthesis. Activation of *de novo* fatty acid biosynthesis regulated by SREBP1c might play an important role in the anti-aging and lifespan extension by caloric restriction.

Key words: caloric restriction, aging, lipid metabolism, adipose tissue remodeling, SREBP1c

Biochemical and Biophysical Research Communications 421 (2012) 15–19

Contents lists available at SciVerse ScienceDirect

Biochemical and Biophysical Research Communications

journal homepage: www.elsevier.com/locate/ybbrc

Reversible induction of PARP1 degradation by p53-inducible cis-imidazoline compounds

Wataru Nagai [1], Naoyuki Okita [*,1], Hiroshi Matsumoto, Hitoshi Okado, Misako Oku, Yoshikazu Higami [*]

Department of Molecular Pathology and Metabolic Disease, Faculty of Pharmaceutical Sciences, Tokyo University of Science, Yamazaki 2641, Noda, Chiba 278-0022, Japan

ARTICLE INFO

Article history:
Received 16 March 2012
Available online 23 March 2012

Keywords:
Nutlin3a
Nutlin3b
Caylin2
Poly(ADP-ribose) polymerase1
p53
MDM2
Proteasome

ABSTRACT

PARP1 is an important enzyme involved in various patho-physiological phenomena such as ischemia/reperfusion (I/R) injury, which occurs when blood flow is restored after cerebral infarction, myocardial infarction and transplantation of various organs. I/R-induced PARP1 over-activation is mediated by production of reactive oxygen species and is involved in NF-κB transactivation. For these reasons, PARP1 is an attractive target for strategies to protect against I/R injury. We previously reported that an MDM2 inhibitor Nutlin3a, a cis-imidazoline compound, induces PARP1 degradation in a p53 and proteasome-dependent manner. In this study, we evaluated the effect of Nutlin3a analogs, Nutlin3b and Caylin2, on PARP1 degradation. Like Nutlin3a, Caylin2, but not Nutlin3b, induced PARP1 degradation in both 3T3-L1 and 3T3-F442A. This result occurred almost in parallel with p53 accumulation. Furthermore Caylin2-induced PARP1 degradation was not observed in p53 deficient mouse embryonic fibroblasts or in the presence of the proteasome inhibitor MG132. These results suggest that Caylin2 induces PARP1 degradation by the same mechanism as Nutlin3a. Finally, we showed that Nutlin3a or Caylin2 treatment induces reversible PARP1 down-regulation without an inflammatory response. For protection against I/R injury, our results support the usability of the p53 inducible cis-imidazoline compounds, Nutlin3a and its analogs, as PARP1 inhibitors.

1. Introduction

Poly(ADP-ribosyl)ation, which is the post-translational protein modification, is involved in cell replication, DNA repair, cell death, and inflammation [1,2]. PARP1 is the most abundant PARP family member in cells, and is dramatically activated by DNA breaks. Therefore, massive DNA damage induces over-activation of PARP1, and then decreases ATP levels via over-consumption of cellular NAD^+, which is required for the ATP production in glycolysis and TCA cycle pathways. It has been also reported that PARP1 over-activation is involved in ischemia/reperfusion (I/R) injury, which occurs during the restoration of blood flow after cerebral infarction, myocardial infarction and organ transplantation [3–5]. For these reasons, PARP1 is an attractive target for protection against I/R injury [6].

We previously reported that Nutlin3a, an MDM2 ubiquitin ligase antagonist, induces p53 and proteasome-dependent PARP1 protein degradation [7]. It has been thought that Nutlin3a is a candidate for anti-tumor drugs, because MDM2 inhibition by Nutlin3a induces p53 stabilization, followed by p53-dependent apoptosis in tumor cells [8]. The discovery of Nutlin3a-induced PARP1 degradation prompted the use of Nutlin3a as a PARP1 inhibitor. Furthermore, considering that p53 has the potential to up-regulate anti-oxidant and anti-inflammatory genes [9–11], Nutlin3a may be a potent anti-I/R drug that has multiple points of action. However, the Nutlin3a pharmacophore that induce PARP1 protein degradation has not been identified. In the present study, to clarify whether Nutlin3a analogs were also able to induce PARP1 protein degradation in a manner similar to Nutlin3a, we examined the effect on PARP1 degradation by the commercially available Nutlin3a enantiomer, Nutlin3b [12,13], and by the Nutlin3a derivative, Caylin2 [14]. Furthermore, by using compounds possessing PARP1 degradation activity, we evaluated the reversibility of PARP1 degradation and the effect on anti-inflammatory IL6 gene expression.

2. Materials and methods

2.1. Cell culture and drugs

Mouse fibroblast 3T3-L1 and 3T3-F442A cell lines were purchased from the RIKEN Bioresource Center (Japan) and the European Collection of Animal Cell Cultures (UK), respectively. The cells were maintained in Dulbecco's modified Eagle's medium (DMEM, low glucose) (WAKO, Japan) with 10% fetal calf serum

* Corresponding authors. Fax: +81 4 7124 3676.
E-mail addresses: nokita7@rs.noda.tus.ac.jp (N. Okita), higami@rs.noda.tus.ac.jp (Y. Higami).
[1] These authors equally contributed to this work.

0006-291X/$ - see front matter © 2012 Elsevier Inc. All rights reserved.
http://dx.doi.org/10.1016/j.bbrc.2012.03.091

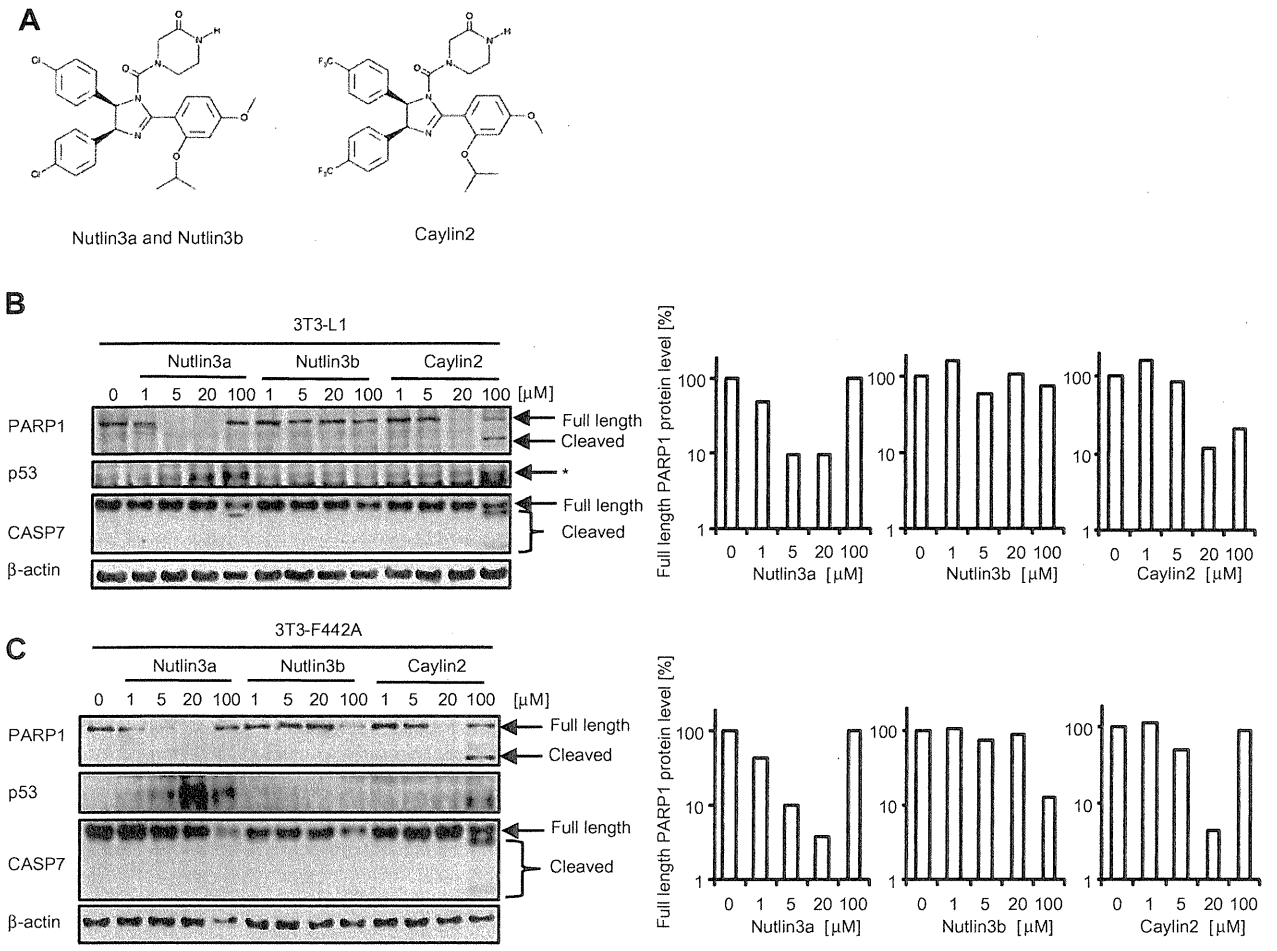

Fig. 1. Caylin2 but not Nutlin3b decreases in PARP1 protein levels in mouse fibroblasts. (A) Structures of Nutlin3a, Nutlin3b, and Caylin2. Mouse fibroblast 3T3-L1 (B) or 3T3-F442A (C) were treated with the indicated concentrations of Nutlin3a, Nutlin3b or Caylin2 for 8 h. The cell lysates were analyzed by Western blotting using the indicated antibodies (left pannel). Quantitative data are shown (right panel). In the p53 panel, the arrow and asterisk show the p53 and nonspecific bands, respectively. All experiments were performed at least three times, and representative data is shown.

and 1% penicillin/streptomycin (Sigma). p53+/+ or −/− MEFs were prepared as described previously [7]. The established MEFs were maintained in DMEM (high glucose) with 10% FCS, 0.1 mM 2-mercaptoethanol, and 1% penicillin/streptomycin. The proteasome inhibitor MG132 was purchased from WAKO (Japan). Nutlin3a, Nutlin3b, and Caylin2 were supplied by Cayman (USA).

2.2. Western blotting

Cell preparation and Western blotting were performed as described previously [7]. As primary antibodies, anti-PARP1 (clone C-2-10, WAKO, Japan), anti-p53 (clone Ab-1, Calbiochem, USA), anti-β actin (clone AC-15, SIGMA, USA), or anti-CASP7 (clone 1F3, MBL, Japan) antibodies were used. For secondary antibodies, horseradish peroxidase-conjugated $F(ab')_2$ fragment of goat anti-mouse IgG or anti-rabbit IgG (Jackson Immunoresearch, USA) were used. The specific proteins were visualized with ImmunoStar LD reagent (WAKO, Japan) and LAS3000 (Fuji Film, Japan), and the data were analyzed using MultiGauge software (Fuji Film, Japan).

2.3. RNA purification and RT-PCR

RNA purification and RT-PCR were performed using RNAiso PLUS, FastPure RNA kit, PrimeScript Reverse Transcriptase and random hexamers (all from TaKaRa, Japan) as described previously [7]. The PCR was performed using Platinum Taq DNA Polymerase High Fidelity (Invitrogen, USA) and primers for *TNFα* (forward, 5′-CCCTCACACTCAGATCATCTTCTC-3′; reverse, 5′-GCCTTGTCCCTTGAAGAGAACC-3′) *IL6* (forward, 5′-GCCTTCCCTACTTCACAAGTCC-3′; reverse, 5′-CAGAATTGCCATTGCACAAC-3′), or *TBP* (forward, 5′-CAGTACAGCAATCAACATCTCAGC-3′; reverse, 5′-CAAGTTTACAGCCAAGATTCACG-3′) as follows: initiation step, at 94 °C for 1 min; amplification step, at 94 °C for 1 min, at 60 °C for 15 s, at 68 °C for 15 s; termination step, 68 °C 15 s. PCR products were subjected to 1.8% agarose gel electrophoresis, stained with ethidium bromide, and visualized with LAS3000. The data was analyzed using MultiGauge software (Fuji Film, Japan).

3. Results

3.1. Caylin2. but not Nutlin3b induces a decrease in PARP1 protein levels in mouse fibroblast cell lines

Although we previously reported that Nutlin3a induces PARP1 protein degradation, we did not address whether Nutlin3a analogs also have the potential to induce PARP1 degradation [7]. Here, we investigated the inducibility of PARP1 degradation by two such analogs, Nutlin3b and Caylin2 in mouse fibroblast cell lines

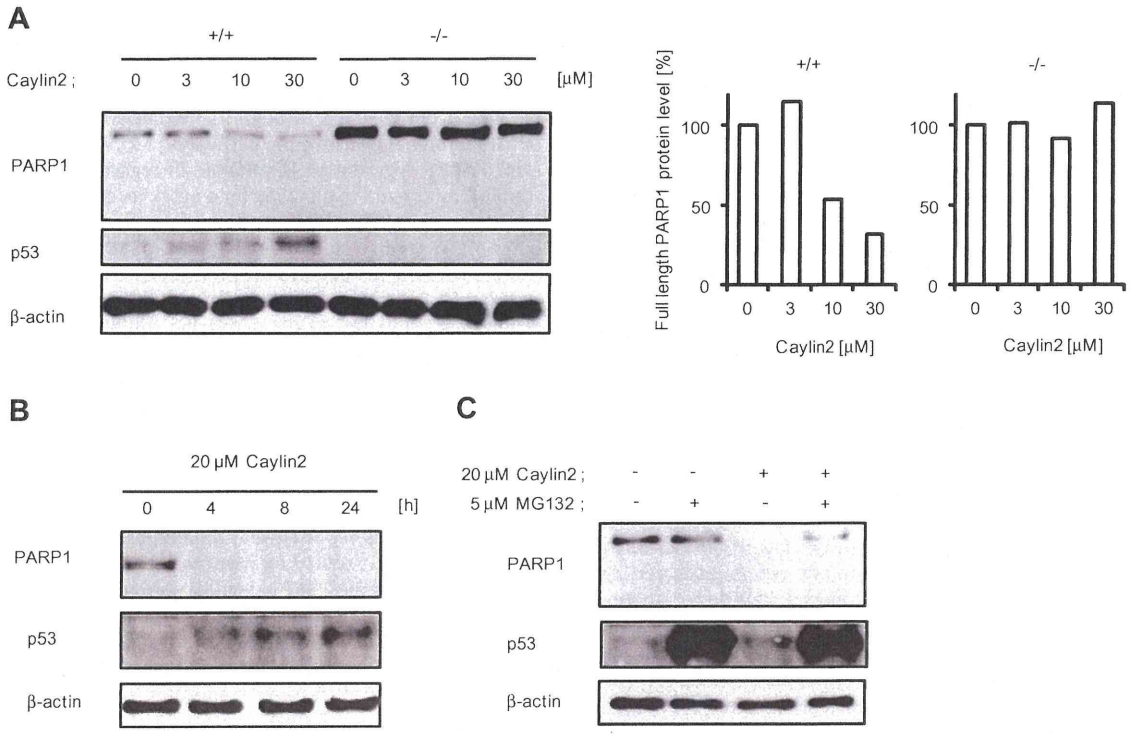

Fig. 2. Caylin2-induced PARP1 degradation is p53 status and proteasome-dependent. (A) p53+/+ and p53−/− MEFs were treated with the indicated concentrations of Caylin2 for 8 h. Cell lysates were analyzed by Western blotting using the indicated antibodies (left panel). Quantitative data are shown (right panel). Each 2 to 3 clones of p53+/+ and p53−/− MEFs were analyzed and representative data are shown. (B) 3T3-L1 cells were treated with 20 μM Caylin2 for the indicated times. The proteins were subjected to Western blotting. (C) 3T3-L1 cells were treated with 20 μM Caylin2 in the presence or absence of 5 μM MG132 proteasome inhibitor (MG) for 8 h, and cell lysates were then subjected to Western blotting using the indicated antibodies.

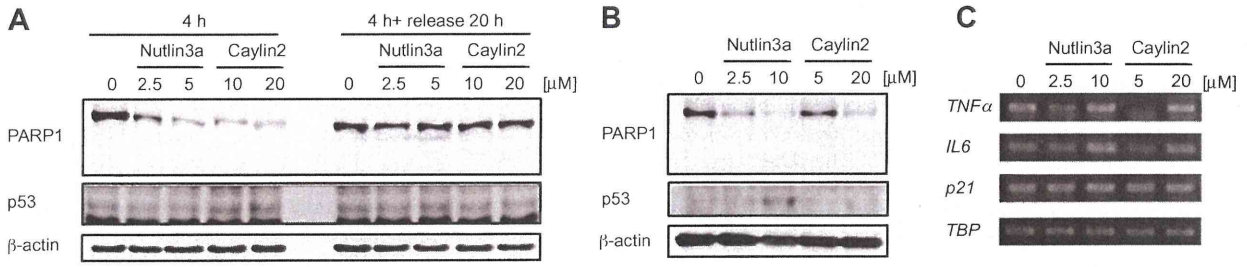

Fig. 3. Nutlin3a or Caylin2 treatment induces reversible PARP1 down-regulation without an inflammatory response. (A) 3T3-L1 cells were treated with Nutlin3a (2.5 or 5 μM) or Caylin2 (10 or 20 μM) for 4 h. After these treatments, cells were also cultured in normal growth medium without treatment for a further 20 h. The cell lysates were analyzed by Western blotting using the indicated antibodies. (B, C) 3T3-L1 cells were treated with 2.5 μM Nutlin3a or 5 μM Caylin2 for 4 h. The protein and RNA expression were analyzed by Western blotting (B) or RT-PCR (C).

(Fig. 1). Nutlin3b is an inactive enantiomer of Nutlin3a, whereas Caylin2 is a Nutlin3a derivative in which trifluoromethyl groups are substituted for chlorine on the 2 phenyl rings (Fig. 1A) [8,12]. As shown in Fig. 1B and C, for both cell lines, 1–20 μM Nutlin3a treatment markedly decreased PARP1 protein levels in a dose dependent manner, whereas 100 μM Nutlin3a treatment had no effect, as per our previous report. p53 accumulation was dose dependent, increasing with the concentration range. Additionally, after 100 μM Nutlin3a-treated, both cell lines were detached from the culture dish and appeared to die without significant CASP7 activation. This observation was consistent with our previous data [7]. Nutlin3b treatment did not markedly alter p53 protein levels in either cell line. In 3T3-L1 cells, Nutlin3b treatment did not affect PARP1 protein level (Fig. 1B). On the other hand, in 3T3-F442A cells, only 100 μM Nutlin3b treatment decreased the PARP1 protein level (Fig. 1C). Similar to the Nutlin3a treatment, 100 μM Nutlin3b-treated cells seemed to die without significant CASP7 activation. Interestingly, Caylin2 treatment showed a signature profile of PARP1 protein in both cell lines. 20 μM Caylin2 treatment induced a significant decrease in PARP1 protein and 100 μM Caylin2 treatment induced PARP1 cleavage, which is considered as an apoptotic hallmark as well as activation of apoptotic caspases such as CASP2, 3, 6, 7, 9, and 10 [15–17]. Indeed, a trypan blue exclusion assay showed that Caylin2-treated cells were viable at 20 μM and dead at 100 μM (Supplemental Fig. 1).

3.2. PARP1 down-regulation by Caylin2 treatment is p53 and proteasome-dependent

Since we previously reported that Nutlin3a-induced PARP1 degradation occurs in a p53 and proteasome dependent manner, we sought to confirm using the same methods as our previous report whether Caylin2-induced PARP1 degradation is inhibited by p53 depletion or proteasome inhibition. As shown in Fig. 2A, p53 WT MEFs, but not p53 KO MEFs, displayed decreasing PARP1 protein levels in a Caylin2 dose dependent manner. Furthermore, as shown in Fig. 2B, Caylin2-induced PARP1 degradation was inhibited by co-treatment with the proteasome inhibitor MG132. These results indicate that Caylin2, like Nutlin3a, induces PARP1 degradation in a p53 and proteasome-dependent manner.

3.3. Nutlin3a or Caylin2 treatment induces reversible PARP1 down-regulation without an inflammatory response

Since PARP1 plays roles in the maintenance of cellular homeostasis through various signal transduction pathways [1,2], reversible down-regulation of the PARP1 protein level is important to protect tissues from I/R injury. Therefore we investigated the reversibility of Nutlin3a- or Caylin2-induced PARP1 degradation. 3T3-L1 cells were treated with Nutlin3a (2.5 or 5 μM) or Caylin2 (10 or 20 μM) for 4 h, and then cultured for 20 h. After 4 h of Nutlin3a or Caylin2 treatment (transient treatment), PARP1 protein levels decreased, although p53 protein levels were not markedly altered (Fig. 3A). After release from those treatments (+20 h), PARP1 protein levels were recovered (Fig. 3A). These results show that Nutlin3a or Caylin2-induced PARP1 degradation is reversible. As it has been reported that Nutlin3a-induced p53 activation leads to up-regulation of inflammatory cytokines [18], we also investigated the influence on inflammation by the transient Nutlin3a or Caylin2 treatment (Fig. 3B). 3T3-L1 cells were treated with the indicated doses of Nutlin3a or Caylin2 for 4 h, and then analyzed the TNFα and IL6 inflammatory genes by RT-PCR. Under these conditions, Nutlin3a or Caylin2 treatment induced PARP1 degradation in a dose dependent manner. Interestingly, we observed different inflammatory responses under these condition (Fig. 3C). The higher dose treatments of Nutlin3a or Caylin2 significantly induced IL6 mRNA expression. However, these doses had little effect or only slightly induced TNFα mRNA expression. On the other hand, the lower dose treatments of Nutlin3a or Caylin2, which were capable of inducing PARP1 degradation, inhibited TNFα mRNA expression and did not affect or only slightly inhibited IL6 mRNA expression. Taken together with Fig. 3B and C, these results indicate that the lower dose treatment of Nutlin3a or Caylin2 has the potential to induce PARP1 degradation without inducing an inflammatory response.

4. Discussion

In this study, we examined the effect of treatment by Nutlin3a analogs on PARP1 protein levels. We demonstrated that Caylin2 induces PARP1 degradation in a similar manner to Nutlin3a. Taken together with our previous study, these results indicate that p53-inducible cis-imidazoline compounds have the potential to induce PARP1 degradation. In the context of using Nutlin3a, Caylin2 and related derivatives as "PARP1 degradation inducers" for I/R injury therapy, a major advantage of this study is that it has demonstrated that Nutlin3a- or Caylin2-induced PARP1 degradation is reversible (Fig. 3A). I/R injury is the tissue damage that occurs during the ischemic and reperfusion period, and as such commonly occurs as a result of ischemic infarction and its treatment or during organ transplantation. In the injured tissues, PARP1 is over-activated by reactive oxygen-mediated DNA damage, resulting in decreases in ATP levels via over-consumption of cellular NAD^+ [1,2]. Therefore, PARP1 inhibition has protective effects on I/R injury. Furthermore, PARP1 itself plays roles in the maintenance of cellular homeostasis through its involvement in the regulation of various signal transduction pathways [1,2]. Taken together, transient PARP1 degradation is valuable in regard to both protection from I/R injury and to allowing for a quick recovery from the harmful effects of PARP1 inhibition. There have been some previous reports of IL6 regulation by p53 or PARP1. p53 has been reported to repress not only IL6 but also the promoter activity of NF-κB, a transcriptional factor of various inflammatory genes including IL6 [10,11]. Additionally, PARP1 activation inhibits the DNA-binding activity of NF-κB [19]. In this study, we showed that Nutlin3a or Caylin2 causes differential effects on inflammatory responses depending on the magnitude of the doses used (Fig. 3C). Our results suggest that the choice of appropriate doses and timing of treatments would be critical to obtain only the beneficial effects on PARP1 degradation when using Nutlin3a or Caylin2 for protection from I/R injury.

Recently, it was reported that inflammasome activation of cardiac fibroblasts is essential for myocardial I/R [20]. So far, our work has revealed that the PARP1 degradation pathway functions efficiently in fibroblast cell lines [7]. These findings support the possibility of practical use of this PARP1 degradation pathway. Further research will require several lines of investigation. Firstly, it will be interesting to identifiy the stereocenter that specifically induces PARP1 degradation. The chiral separation of Nutlin3 (Nutlin3a and Nutlin3b) has been achieved, although the absolute stereocenter has not been known [12,13]. In Caylin2 the chiral separation has not been achieved. We predict that Caylin2a (Caylin2 of Nutlin3a type), but not Caylin2b (Caylin2 of Nutlin3b type), may be the potential to induce PARP1 degradation and are performing further analyses now. Secondly, it will be important to explore PARP1 degradation inducers that different structures than the cis-imidazoline compounds such as Nutlin3a or Caylin2. Thus, elucidation of the mechanism of reversible PARP1 degradation induction is important for the optimization of compounds which induce this phenomenon, resulting in the establishment of selective chemotherapeutic strategies against I/R injury.

Acknowledgments

The authors thank Dr. Susumu Kobayashi (Tokyo University of Science, Japan) and Dr. Takahiro Suzuki (Tokyo University of Science, Japan) for their valuable expertise and all members of Higami laboratory for their cooperation. This work was supported by Grant-in-Aid for Young Scientists (B) from the Ministry of Education, Culture, Sports, Science and Technology (23790201) (N.O.) and partially by Challenging Exploratory Research from the Ministry of Education, Culture, Sports, Science and Technology (23659207) (Y.H.). RIDAI SCITEC holds a patent (PCT/JP2012/052565) on the method of treating ischemia/reperfusion injury, and N.O., and Y.H. are the inventors of the patent.

References

[1] M. Masutani, H. Nakagama, T. Sugimura, Poly(ADP-ribosyl)ation in relation to cancer and autoimmune disease, Cell. Mol. Life Sci. 62 (2005) 769–783.
[2] M. Miwa, M. Masutani, PolyADP-ribosylation and cancer, Cancer Sci. 98 (2007) 1528–1535.
[3] H.K. Eltzschig, T. Eckle, Ischemia and reperfusion – from mechanism to translation, Nat. Med. 17 (2011) 1391–1401.
[4] S.J. van Wijk, G.J. Hageman, Poly(ADP-ribose) polymerase-1 mediated caspase-independent cell death after ischemia/reperfusion, Free Radic. Biol. Med. 39 (2005) 81–90.
[5] P. Pacher, C. Szabo, Role of the peroxynitrite-poly(ADP-ribose) polymerase pathway in human disease, Am. J. Pathol. 173 (2008) 2–13.

[6] D.V. Ferraris, Evolution of poly(ADP-ribose) polymerase-1 (PARP-1) inhibitors, from concept to clinic, J. Med. Chem. 53 (2010) 4561–4584.
[7] S. Matsushima, N. Okita, M. Oku, W. Nagai, M. Kobayashi, Y. Higami, An Mdm2 antagonist, Nutlin-3a, induces p53-dependent and proteasome-mediated poly(ADP-ribose) polymerase1 degradation in mouse fibroblasts, Biochem. Biophys. Res. Commun. 407 (2011) 557–561.
[8] L.T. Vassilev, B.T. Vu, B. Graves, D. Carvajal, F. Podlaski, Z. Filipovic, N. Kong, U. Kammlott, C. Lukacs, C. Klein, N. Fotouhi, E.A. Liu, In vivo activation of the p53 pathway by small-molecule antagonists of MDM2, Science 303 (2004) 844–848.
[9] A.A. Sablina, A.V. Budanov, G.V. Ilyinskaya, L.S. Agapova, J.E. Kravchenko, P.M. Chumakov, The antioxidant function of the p53 tumor suppressor, Nat. Med. 11 (2005) 1306–1313.
[10] U. Santhanam, A. Ray, P.B. Sehgal, Repression of the interleukin 6 gene promoter by p53 and the retinoblastoma susceptibility gene product, Proc. Natl. Acad. Sci. USA 88 (1991) 7605–7609.
[11] E.A. Komarova, V. Krivokrysenko, K. Wang, N. Neznanov, M.V. Chernov, P.G. Komarov, M.L. Brennan, T.V. Golovkina, O.W. Rokhlin, D.V. Kuprash, S.A. Nedospasov, S.L. Hazen, E. Feinstein, A.V. Gudkov, p53 is a suppressor of inflammatory response in mice, FASEB J. 19 (2005) 1030–1032.
[12] Z. Wang, M. Jonca, T. Lambros, S. Ferguson, R. Goodnow, Exploration of liquid and supercritical fluid chromatographic chiral separation and purification of Nutlin-3 – a small molecule antagonist of MDM2, J. Pharm. Biomed. Anal. 45 (2007) 720–729.
[13] Cayman Chemical, http://www.caymanchem.com/app/template/Product.vm/catalog/10009816.
[14] Cayman Chemical, http://www.caymanchem.com/app/template/Product.vm/catalog/10005002.
[15] S.H. Kaufmann, S. Desnoyers, Y. Ottaviano, N.E. Davidson, G.G. Poirier, Specific proteolytic cleavage of poly(ADP-ribose) polymerase: an early marker of chemotherapy-induced apoptosis, Cancer Res. 53 (1993) 3976–3985.
[16] Y.A. Lazebnik, S.H. Kaufmann, S. Desnoyers, G.G. Poirier, W.C. Earnshaw, Cleavage of poly(ADP-ribose) polymerase by a proteinase with properties like ICE, Nature 371 (1994) 346–347.
[17] C. Pop, G.S. Salvesen, Human caspases: activation, specificity, and regulation, J. Biol. Chem. 284 (2009) 21777–21781.
[18] B. Huang, D. Deo, M. Xia, L.T. Vassilev, Pharmacologic p53 activation blocks cell cycle progression but fails to induce senescence in epithelial cancer cells, Mol. Cancer Res. 7 (2009) 1497–1509.
[19] W.J. Chang, R. Alvarez-Gonzalez, The sequence-specific DNA binding of NF-kappa B is reversibly regulated by the automodification reaction of poly(ADP-ribose) polymerase 1, J. Biol. Chem. 276 (2001) 47664–47670.
[20] M. Kawaguchi, M. Takahashi, T. Hata, Y. Kashima, F. Usui, H. Morimoto, A. Izawa, Y. Takahashi, J. Masumoto, J. Koyama, M. Hongo, T. Noda, J. Nakayama, J. Sagara, S. Taniguchi, U. Ikeda, Inflammasome activation of cardiac fibroblasts is essential for myocardial ischemia/reperfusion injury, Circulation 123 (2011) 594–604.

G Model
MAD 10573 1–12

ARTICLE IN PRESS

Mechanisms of Ageing and Development xxx (2012) xxx–xxx

Contents lists available at SciVerse ScienceDirect

Mechanisms of Ageing and Development

journal homepage: www.elsevier.com/locate/mechagedev

Differential responses of white adipose tissue and brown adipose tissue to caloric restriction in rats

Naoyuki Okita[a,1], Yusuke Hayashida[a,1], Yumiko Kojima[a,1], Mayumi Fukushima[a], Keiko Yuguchi[a], Kentaro Mikami[a], Akiko Yamauchi[a], Kyoko Watanabe[a], Mituru Noguchi[b], Megumi Nakamura[c], Toshifusa Toda[c], Yoshikazu Higami[a,*]

[a] Molecular Pathology & Metabolic Disease, Faculty of Pharmaceutical Sciences, Tokyo University of Science, Tokyo, Japan
[b] Department of Urology, Faculty of Medicine, Saga University, Japan
[c] TMIG Proteomics Collaboration Center, Tokyo Metropolitan Institute of Gerontology, Tokyo, Japan

ARTICLE INFO

Article history:
Received 30 August 2011
Received in revised form 14 December 2011
Accepted 22 February 2012
Available online xxx

Keywords:
Caloric restriction
Adipose tissue
Proteome analysis
Mitochondrial biogenesis
Fatty acid biosynthesis
Mitochondrial biogenesis

ABSTRACT

Caloric restriction (CR) slows the aging process and extends longevity, but the exact underlying mechanisms remain debatable. It has recently been suggested that the beneficial action of CR may be mediated in part by adipose tissue remodeling. Mammals have two types of adipose tissue: white adipose tissue (WAT) and brown adipose tissue (BAT). In this study, proteome analysis using two-dimensional gel electrophoresis combined with MALDI-TOF MS, and subsequent analyses were performed on both WAT and BAT from 9-month-old male rats fed *ad libitum* or subjected to CR for 6 months. Our findings suggest that CR activates mitochondrial energy metabolism and fatty acid biosynthesis in WAT. It is likely that in CR animals WAT functions as an energy transducer from glucose to energy-dense lipid. In contrast, in BAT CR either had no effect on, or down-regulated, the mitochondrial electron transport chain, but enhanced fatty acid biosynthesis. This suggests that in CR animals BAT may change its function from an energy consuming system to an energy reservoir system. Based on our findings, we conclude that WAT and BAT cooperate to use energy effectively *via* a differential response of mitochondrial function to CR.

1. Introduction

Mammals have two types of adipose tissue, white adipose tissue (WAT) and brown adipose tissue (BAT), which can be distinguished by their morphology and function (Saely et al., 2010). WAT is a major tissue for energy storage in the form of triglycerides (TG). It consists predominantly of white adipocytes that store energy in TG-containing unilocular droplets. Several WAT-derived secretory molecules (adipokines), such as adiponectin, leptin and pro-inflammatory cytokines including tumor necrosis factor α (TNFα), have been characterized. Adiponectin enhances insulin sensitivity and fatty acid oxidation *via* the cellular fuel sensor AMP-activated protein kinase (AMPK). Moreover, it acts as an anti-inflammatory and anti-atherogenic adipokine (Stofkova, 2009; Yamauchi et al., 2001, 2002). Leptin reduces appetite and enhances energy expenditure *via* the hypothalamus/sympathetic nervous system, and also functions as a pro-inflammatory adipokine (Stofkova, 2009). TNFα promotes insulin resistance (Hotamisligil et al., 1995). Thus, several adipokines are involved in energy homeostasis, insulin resistance and inflammation (Gnacińska et al., 2009; Torres-Leal et al., 2010). It is well known that white adipocytes alter their characteristics with their size. Large hypertrophic adipocytes, possessing more TG, secrete less adiponectin and more pro-inflammatory cytokines including leptin, while small adipocytes, which have less TG, secrete more adiponectin and less pro-inflammatory adipokines (DeClercq et al., 2008). Moreover, small adipocytes are generally found to be more sensitive to insulin and act as powerful buffers, absorbing lipids in the postprandial period. If this buffering action is impaired, extra adipose tissues can accumulate lipids in the form of TG, resulting in insulin resistance (Frayn, 2002). Small adipocytes are therefore considered more beneficial for a healthy lifespan than large ones (Higami et al., 2005; Zhu et al., 2007).

In contrast to WAT, BAT plays an important role in energy expenditure. It predominantly consists of mitochondria-rich brown adipocytes, which have multilocular lipid droplets and express the BAT-specific mitochondrial protein, Uncoupling Protein 1 (UCP1; Farmer, 2008; Saely et al., 2010). UCP1 uncouples mitochondrial ATP synthesis from electron transport chain

* Corresponding author at: Molecular Pathology & Metabolic Disease, Faculty of Pharmaceutical Sciences, Tokyo University of Science, 2641 Yamazaki, Noda, Chiba 278-8510, Japan. Tel.: +81 4 7121 3676; fax: +81 4 7121 3676.
E-mail address: higami@rs.noda.tus.ac.jp (Y. Higami).
[1] These authors contributed equally to this work.

0047-6374/$ – see front matter © 2012 Elsevier Ireland Ltd. All rights reserved.
doi:10.1016/j.mad.2012.02.003

activity, and is responsible for energy expenditure *via* heat production. BAT is highly vascularized and innervated by the sympathetic nervous system. It is a major site of both cold- and diet-induced thermogenesis, particularly in small rodents (Farmer, 2008; Saely et al., 2010). Recent studies using positron-emission tomography have identified BAT in human adults, and shown that its activity correlates inversely with body mass index. Active BAT therefore appears to play an important role in the control of body temperature and adiposity in humans (Saely et al., 2010).

Recently, new genetic interventions that extend mammalian lifespan have emerged (Kenyon, 2005). Caloric restriction (CR), however, remains the most robust, reproducible and simple experimental manipulation known to extend both median and maximum lifespan, and to retard several age-related pathophysiological changes in laboratory rodents (Masoro, 2005; Sinclair, 2005; Weindruch and Walford, 1988; Yu, 1994). The anti-aging and/or pro-longevity effects of CR have been observed in several species, from yeast to laboratory rodents (Masoro, 2005; Sinclair, 2005). Recent studies suggest that CR is effective in non-human primates as well (Colman et al., 2009). It is widely accepted that suppression of the growth hormone (GH)/insulin-like growth factor (IGF-1) signal, attenuation of oxidative and other stresses, modulation of glycemia and insulinemia, enhanced mitochondrial biogenesis and activation of sirtuins may be significant factors in the actions of CR, but the exact underlying mechanisms are still debatable (Masoro, 2005; Sinclair, 2005). It has been reported that fat-specific insulin receptor knockout (FIRKO) mice live longer than their controls (Blüher et al., 2003). These mice reduce adiposity and enhance mitochondrial biogenesis with altered secretion of adipokines, including higher adiponectin and lower pro-inflammatory cytokines (Blüher et al., 2002; Katic et al., 2007). The transcription factors C/EBPα, C/EBPβ and peroxisome proliferator-activated receptor γ (PPARγ) are master regulators of adipocyte differentiation (Farmer, 2006). Mice in which C/EBPα was replaced with C/EBPβ (β/β mice) live longer and have reduced adiposity (Chiu et al., 2004). In contrast, the hetero-deficiency PPARγ knockout (KO) mice have a shorter lifespan (Argmann et al., 2009). Transgenic mice expressing adiponectin in the liver live longer than controls and show reduced high-calorie diet-induced obesity (Otabe et al., 2007). These results show that altered gene expression in the adipose tissue, and modulation of adipokine secretion, can influence the lifespan of rodents. CR reduces adiposity by altering the gene expression profile (Higami et al., 2004, 2006a), and lowering plasma insulin and leptin levels, as well as raising plasma adiponectin levels (Yamaza et al., 2007; Zhu et al., 2007). CR also reverses age-associated insulin resistance, possibly through decreased adiposity (Barzilai et al., 1998). Moreover, in mice, CR promotes mitochondrial biogenesis in both WAT and BAT, and it has been suggested that PPARγ co-activator 1α (PGC1α), Sirt1 and Sirt3 are key players in CR-enhanced mitochondrial biogenesis (Anderson and Prolla, 2009; Nisoli et al., 2005; Shi et al., 2005). Therefore, we hypothesized that the beneficial actions of CR may be partially mediated by functional alteration of WAT and BAT. Proteome analysis of WAT from 24-month-old rats fed *ad libitum* (AL) or subjected to CR was recently reported (Valle et al., 2010). However, to our knowledge analysis of the effects of CR in both WAT and BAT at a young age, and a comparison of these effects, has not yet been reported.

In this study, to understand the molecular basis of CR-associated metabolic alterations in adipose tissues, we performed histological examination and proteome analysis of both WAT and BAT from 9-month-old male rats fed AL or subjected to CR for 6 months, and the responses to CR were compared between WAT and BAT. This enabled differential and similar responses to CR between both tissues to be identified.

2. Materials and methods

2.1. Animals and diet

The present study was conducted in accordance with the provisions of the Ethics Review Committee for Animal Experimentation at Tokyo University of Science. Male Wistar rats aged 5–7 weeks were purchased from Clea Inc. (Tokyo, Japan) and were maintained under SPF conditions at 23 °C and a 12 h light–dark cycle, in the Laboratory Animal Center at the Faculty of Pharmaceutical Sciences, Tokyo University of Science. All rats were provided with water and fed *ad libitum* with a Labo MR Stock diet (NOSAN, Yokohama, Japan).

From 12 weeks of age, rats were divided into two groups: one was fed *ad libitum* (AL) and the other was calorie restricted (CR, 70% of the *ad libitum* energy intake). CR rats were fed every other day (Higami et al., 2006b). Their 2-day food allotment was equal to 140% of the mean daily intake of AL rats. At 9 months of age, all rats were sacrificed under anesthesia with isoflurane inhalation (Mylan, Canonsburg, PA, USA) 3–5 h after turning on the lights. Prior to sacrifice, CR and AL groups were further divided into two treatments (fed or fasted) as follows. CR-fed rats were provided with food 30 min prior to turning off the lights in the evening, and were sacrificed the following morning. CR-fasted rats were fasted overnight for approximately 16 h prior to sacrifice. To evaluate the effect of fasting, half of the AL rats were sacrificed 16 h after the removal of food, which occurred when the lights were turned off (AL-fasted), while the other half were sacrificed without removing the food (AL-fed). Mean body weight data (±SEM) of AL-fasted and CR-fasted rats are shown in Table 1. When the animals were sacrificed, both epididymal WAT and interscapular BAT were collected and their weights measured (Table 1). A sub-sample of the isolated WAT and BAT were fixed in a buffered formalin solution for histological examination, and the rest was immediately diced, frozen in liquid nitrogen, and stored at −80 °C.

2.2. Histological examination

Fixed tissues were processed routinely, embedded in paraffin, and sectioned. 5 μm sections were stained with hematoxylin–eosin. Stained sections were scanned by microscopy with a CCD camera (Nikon, Tokyo, Japan). The size distribution of each white area in the black-and-white images, which indicates a lipid droplet, was measured and calculated using "ImageJ 1.43u/Java1.6.0_22" software. To avoid inter-rating variation, a single observer (Yu. H.) carried out the morphometric analysis.

2.3. Analysis of triglyceride (TG) contents

Total lipid was extracted from WAT and BAT of AL-fasted and CR-fasted rats, and the triglyceride (TG) content was measured using a LabAssay™ Triglyceride kit (Wako, Osaka, Japan), according to a previous report (Higami et al., 2006a) and the manufacturer's instructions. The TG content per 100 mg protein was calculated.

2.4. Two-dimensional gel electrophoresis (2-DE)

Two-dimensional gel electrophoresis (2-DE) using the IPG-DALT system and subsequent MALDI-TOF MS analysis were performed as previously described (Nakamura et al., 2006). Briefly, to extract total protein, frozen WAT and BAT from AL-fed, AL-fasted, CR-fed and CR-fasted rats were homogenized in extraction buffer containing 5 M urea, 2 M thiourea, 2% (w/v) 3-[(3-cholamidopropyl) dimethylammonio]-1-propanesulfonate (CHAPS), 2% (w/v) sulfobetaine10, 2% Pharmalyte 3-10, 65 mM dithiothreitol (DTT), 1% protease inhibitor cocktail and 1% phosphatase inhibitor cocktail, using a sonicator. Samples were centrifuged at 15,000 rpm, at 20 °C for 30 min, and the supernatants were collected. The supernatant samples were prepared from six animals in each group, and each individual was assessed separately. The protein content of each sample was determined using the Bradford method.

First-dimensional isoelectric focusing (IEF) was carried out on nonlinear immobilized pH gradients (Immobiline DryStrip, pH 3–10 NL, 18 cm long; GE Healthcare, Cleveland, OH, USA). Passive sample application during rehydration was performed by placing the Immobiline DryStrip gel side down overnight in a rehydration tray that contained the sample in the rehydration solution (6 M urea, 2 M thiourea, 13 mM DTT, 1% Pharmalyte 3-10, 2.5 mM acetic acid, 0.0025% Orange G and 2% Triton X-100). As the strip hydrates, proteins in the sample are absorbed

Table 1

	AL	CR
Body weight (g)	523 ± 11	344 ± 9*
WAT weight (g)	7.04 ± 0.464	2.16 ± 0.160*
WAT weight/body weight (%)	1.34 ± 0.078	0.627 ± 0.044*
BAT weight (g)	0.454 ± 0.036	0.255 ± 0.014*
BAT weight/body weight (%)	0.087 ± 0.007	0.074 ± 0.005

* $p < 0.001$ by Student's *t*-test.

Please cite this article in press as: Okita, N., et al., Differential responses of white adipose tissue and brown adipose tissue to caloric restriction in rats. Mech. Ageing Dev. (2012), doi:10.1016/j.mad.2012.02.003

and distributed over the entire length of the strip. The IEF was performed at 20 °C starting at 500 V, with the voltage being gradually increased to 3500 V, using a PowerPhoreStar power supply (Anatech, Tokyo, Japan). After electrofocusing, the gel strips were equilibrated for 45 min with gentle shaking in 5 mL of equilibration buffer (6 M urea, 32 mM DTT, 25 mM Tris–HCl, pH 6.8, 2% SDS, 0.0025% BPB and 30% glycerol). In the second-dimension SDS–PAGE, the equilibrated gel strips were placed on top of 7.5% polyacrylamide gels (18 cm × 20 cm × 1 mm), and run in SDS running buffer (0.1 M Tris, 0.1 M Tricine and 0.1% SDS) until the dye front reached the bottom of the gel. Then, the gel was fixed with fixing solution (10% acetic acid and 50% methanol) and washed with washing solution (7% acetic acid and 10% methanol). Finally, the gel was stained with SYPRO Ruby Protein Gel Stain (Molecular Probe, Eugene, OR, USA) and washed with washing solution (8% acetic acid and 10% methanol) and pure water.

Fluorescent gel images were obtained by scanning with a FluoroPhoreStar 3000 (Anatech) and analyzed with Progenesis PG200 software (Nonlinear Dynamics, Durham, NC, USA). Molecular masses were determined by running standard protein markers, covering the range of 10–250 kDa. The pI values used were those given by the supplier of the IPG strips. After background subtraction, spots from each gel were automatically matched to the spots on a reference gel. To validate automated spot detection and matching, images were edited manually and streaks, speckles and artifacts were removed. The reference gel was obtained using mixed samples from AL-fed and CR-fed rat tissues. For all spot-intensity calculations, normalization volumes were used to calculate relative intensity (RI) for each spot: RI = vi/vt, where vi is the volume (pixel intensities integrated over the area of each spot) of the individual spot, and vt is the sum of the volumes of all matched spots. Only spots displaying a significant change (≥1.4-fold) in their normalized spot intensity were considered for protein identification.

2.5. Matrix-assisted laser desorption/ionization time-of-flight mass spectrometry (MALDI-TOF MS) analysis

For mass spectrometric identification, protein spots on the SYPRO Ruby-stained 2-DE gel were excited and the spots that showed different density were excised with a FluoroPhoreStar3000 gel picker (Anatech). The gel pieces were reduced with 1.5 mg/mL DTT in 100 mM ammonium bicarbonate, alkylated with 10 mg/mL iodoacetamide in 100 mM ammonium bicarbonate, then destained, washed, and finally dried. Subsequently, the gel pieces were digested with 5 μg/mL sequencing grade modified trypsin (Promega, Madison, WI, USA) in a 50 mM ammonium bicarbonate and 30% acetonitrile solution, at 30 °C overnight. The tryptic peptide mixture samples were concentrated in a SpeedVac Vacuum system (Savant Instruments, Holbrook, NY, USA) and were rehydrated with 10 μL of 0.1% trifluoroacetic acid (TFA). The samples were then adsorbed onto a Zip-Tip μC18 column (Millipore, Billerica, MA, USA). The resin was washed with 0.1% TFA and the peptides were eluted with 50% acetonitrile in 0.1% TFA. The elution was analyzed by the peptide mass fingerprint (PMF) method, based on MALDI-TOF MS as follows: 2 μL of tryptic peptides were spotted onto a ready-to-use Shimadzu 384 target plate (Shimadzu, Kyoto, Japan), and mixed with 0.5 μL of matrix solution [53 mM CHCA (α-cyano-4-hydroxycinnamic acid), 50% acetonitrile, 40% methanol and 0.1% TFA]. Mass spectra were collected on an AXIMA-CFR MALDI-TOF instrument (Shimadzu) in reflectron positive ion mode. The instrument was externally calibrated using the calibrant spots on the pre-spotted target. Monoisotopic peaks were generated by Kompact software (Shimadzu), and protein identification was carried out primarily using the PMF Search of Mascot (http://www.matrixscience.com) and the MS-Fit search engine in Protein Prospector (http://prospector.ucsf.edu) by sending a query of the PMF peak list. In some cases, samples were further analyzed by MALDI TOF TOF MS/MS (AXIMA-TOF2; Shimadzu). An MS/MS ion search of Mascot was used for confirmation.

2.6. DNA extraction

Total DNA, including mitochondrial DNA (mtDNA), was extracted from WAT and BAT by digestion with proteinase K and 10% SDS (100 μg/μL) in a buffer containing 150 mM NaCl, 10 mM Tris–HCl, pH 8.0, and 10 mM EDTA. Homogenate samples were incubated overnight at 55 °C, and then an equal volume of phenol was added and samples were rotated for 1 h. After centrifugation, the aqueous phase was removed to a fresh tube and rotated with an equal volume of PCI (phenol/chloroform/isoamyl alcohol) for 1 h. To remove RNA, the aqueous phase was incubated with 0.02 volume of RNase A (Wako, Osaka, Japan) for 1 h at 37 °C. This phenol and PCI procedure was repeated once more. DNA was precipitated from the aqueous phase by adding 0.1 volume of 3 M sodium acetate after adding a double volume of 100% ethanol. The DNA was washed twice with 180 μL of 70% ethanol, air dried gently and re-suspended in TE buffer. The concentration was adjusted to 20 ng/μL.

2.7. Analysis of mtDNA contents

A quantitative PCR assay was performed using the Applied Biosystems 7300 real-time PCR system (Life Technologies, Carlsbad, CA, USA) (Koekemoer et al., 1998). Nuclear DNA and mtDNA were amplified by real-time PCR for solute carrier family 16, member 1 (SLC16A1) and cytochrome c oxidase subunit 2 (COX2), respectively. The primer pairs' sequences for real-time PCR analysis of SLC16A1 and COX2 were: SLC16A1 (forward) 5′-TAG CTG GAT CCC TGA TGC GA-3′, (reverse) 5′-GCA TCA GAC TTC CCA GCT TCC-3′ (32); COX2 (forward) 5′-CTT ACA AGA CGC CAC ATC AC-3′, (reverse) 5′-GAA TTC GTA GGG AGG GAA GG-3′ (Jahnke et al., 2010). Relative amounts of mtDNA were expressed as COX2/SLC16A1.

2.8. Analysis of mitochondrial activities

Activities of citrate synthase (CS) and electron transport chain complex IV, cytochrome c oxidase (Complex IV), were measured as previously reported with some modifications (Alp et al., 1976; Daley et al., 2005). Briefly, WAT and BAT were homogenized in homogenization buffer containing 50 mM Tris–HCl, pH 7.4, 150 mM NaCl, 1% phosphatase inhibitor cocktail, 5 mM EDTA, 1% protease inhibitor cocktail, 1% Triton X-100 and 0.05% sodium deoxycholate. Protein concentration was determined using the BCA protein assay kit (Thermo Scientific, Rockford, IL, USA) according to the manufacturer's protocol.

For CS activity measurements, a reaction mixture containing 0.1 mM 5,5-dithio-bis-(2-nitrobenzoic) acid (Wako), 0.5 mM acetyl-CoA (Wako), 0.1% Triton X-100 and 100 mM Tris–HCl, pH 8.0, with the tissue homogenate was prepared. The homogenates contained 5–8 μg protein from WAT or 0.5–0.8 μg protein from BAT. After incubation at 28 °C for 5 min, the absorbance at 412 nm (SpectraMax Plus384, Molecular Devices, Sunnyvale, CA, USA) was measured for 3 min to determine the nonspecific activity. Reactions were then initiated by addition of 0.5 mM oxaloacetate (Wako) in a final volume of 200 μL, and the change in absorbance was recorded for at least 3 min (Alp et al., 1976).

The activity of Complex IV was measured at 30 °C as the rate of cytochrome c oxidation, using a spectrophotometer (SpectraMax Plus 384, Molecular Devices) at 550 nm (Daley et al., 2005). A cytochrome c solution containing 10 mg/mL reduced cytochrome c (Sigma–Aldrich, St. Louis, MO, USA) and 50 mM Tris–HCl, pH 7.2, was prepared and an excess amount of sodium ascorbate (to saturation) was added. The excess sodium ascorbate was removed on a PD-10 column. The reaction mixture contained 25 μM cytochrome c in 50 mM Tris–HCl, pH 7.2. Reactions were initiated by adding the tissue homogenates (which contained 5.4–41 μg protein from WAT or 0.6–2.3 μg protein from BAT) to the reaction mixture. The final concentration of cytochrome c was 20 μM. The first order rate constant (k) was calculated from the natural logarithms of the absorbance after adding the tissue homogenates. These calculated values were then taken to be (k) and the activity was expressed in k/min/mg protein. Complex IV activities were also measured in the presence of 1 mM potassium ferricyanide as a blank (Daley et al., 2005).

2.9. RNA extraction and real-time reverse transcription-polymerase chain reaction (RT-PCR)

Total RNA was extracted from frozen WAT and BAT using RNAiso PLUS (Takara, Shiga, Japan), and was purified using the FastPure RNA kit (Takara), according to the manufacturer's protocol. To obtain cDNA, 1 μg RNA was subjected to reverse transcription by PrimeScript Reverse Transcriptase (Takara) with random hexamer primers (Takara). Real-time quantitative PCR was performed using the Applied Biosystems 7300 real-time PCR system (Life Technologies) with SYBR Premix ExTaqII (Takara), according to the manufacturer's instructions. Transcripts of PGC1α, Nuclear respiratory factor 1 (NRF1), Transcription factor A, mitochondrial (TFAM), Cytochrome c oxidase IV (COX4), UCP1, Fatty acid synthase (FAS) and TATA box binding protein (TBP) were amplified. TBP was used for normalization. Primer sequences are shown in Table 2.

2.10. Protein extraction and analysis of target protein levels by Western blot

WAT and BAT were lysed with lysis buffer (50 mM Tris–HCl, pH 6.8, 2% SDS and 5% glycerol), boiled for 5 min and sonicated. Protein concentrations of the soluble fraction were determined using the BCA protein Assay Kit, standardized by the addition of lysis buffer, 2-mercaptoethanol and bromophenol blue were added to the proteins to obtain final concentrations of 5% and 0.025%, respectively, and the samples boiled for 5 min. Equal amounts of proteins (5–20 μg) were subjected to SDS–PAGE and transferred to nitrocellulose membranes. Membranes were blocked with 2.5% skim milk and 0.25% BSA in Tris-buffered saline (50 mM Tris, pH 7.4, and 150 mM NaCl) containing 0.1% Tween 20 (TTBS) for 1 h at room temperature, and then probed with the appropriate primary antibodies overnight at 4 °C or for 2 h at room temperature. The primary antibodies for ATP-citrate lyase (Epitomics, Burlingame, CA, USA), ATP-citrate lyase pS455 (Epitomics) and β-actin (Sigma–Aldrich) were used. After washes with TTBS, membranes were incubated with the appropriate secondary antibody (horseradish peroxidase-conjugated $F(ab')_2$ fragment of goat anti-mouse IgG or anti-rabbit IgG; Jackson ImmunoResearch, West Grove, PA, USA), for 1 h at room temperature. After washing with TTBS, the membranes were incubated with ImmunoStar LD reagent (Wako). The specific proteins were visualized with LAS3000 (Fujifilm, Tokyo, Japan), and the data were analyzed using Multigauge software (Fujifilm).

2.11. Statistical analysis

All data derived from three to six rats in each group were expressed as means ± SEM and were examined using Student's t-test or Tukey's t-test. Differences with p values <0.05 were deemed statistically significant.

Please cite this article in press as: Okita, N., et al., Differential responses of white adipose tissue and brown adipose tissue to caloric restriction in rats. Mech. Ageing Dev. (2012), doi:10.1016/j.mad.2012.02.003

Table 2

	Forward	Reverse
PGC1α	5′-AGACGGATTGCCCTCATTTG-3′	5′-CAGGGTTTGTTCTGATCCTGTG-3′
NRF1	5′-TGATGAGGTAACTGCCCATCTG-3′	5′-TTGGAGGGTGAGATGCAGAG-3′
TFAM	5′-CGATTTTCTACAGAACAGCTACCC-3′	5′-GCTCTTTATACTTGCTCACAGCTTC-3′
COX4	5′-CATTTCTACTTCGGTGTGCCTTC-3′	5′-CACATCAGGCAAGGGGTAGTC-3′
UCP1	5′-CAGAGTTATAGCCACCACAGAAAGC-3′	5′-CAGGAGTGTGGTGCAAAACC-3′
FAS	5′-AGCAGGCACACACAATGGAC-3′	5′-GAAGAAGAAAGAGAGCCGGTTG-3′
TBP	5′-CAGTACAGCAATCAACATCTCAGC-3′	5′-CAAGTTTACAGCCAAGATTCACG-3′

PGC1α: peroxisome proliferator activated receptor gamma coactivator 1α; NRF1: nuclear respiratory factor 1; TFAM: mitochondrial transcription factor A; COX4: cytochrome c oxidase 4; UCP1: uncoupling protein 1; FAS: fatty acid synthase; TBP: TATA box binding protein.

3. Results

3.1. Histological analysis and triglyceride (TG) contents

CR markedly reduced body, WAT and BAT weights. CR also lowered the relative weight of WAT, but not of BAT, compared to the body weight (Table 1).

As shown in Fig. 1A and B, CR markedly reduced the size of lipid droplets. Because the unilocular lipid droplet occupies most of the cytoplasm of white adipocytes, the size of the lipid droplet is thought to represent the cell size. The median adipocyte size was 3203 μm^2 in the AL group and 2169 μm^2 in the CR group. The adipocyte size distribution was wider in AL rats compared with CR rats. The percentage of adipocytes that were larger than 8000 μm^2 was 6.6% in AL rats and less than 0.5% in CR rats. In contrast, the portion of adipocytes that were smaller than 2000 μm^2 was approximately 50% in CR rats and 33% in AL rats (Fig. 1A, B and E). Consistent with the histological data, CR significantly reduced TG content in the fasted state (Fig. 1G).

In BAT, brown adipocytes with multilocular lipid droplets of various sizes were observed. Moreover, many white adipocytes had infiltrated into the BAT. In BAT, it is difficult to distinguish the large lipid droplets in brown adipocytes from the white adipocytes that have infiltrated into BAT. Therefore, lipid droplet size is not thought to represent cell size. In contrast to WAT, large lipid droplets were predominantly observed in BAT from CR rats compared with AL rats. The median lipid droplet size was 123 μm^2 in AL rats and 191 μm^2 in CR rats. The proportion of lipid droplets larger than 300 μm^2 was more than 30% in CR rats and approximately 15% in the AL group (Fig. 1C, D and F). Consistent with the histological data, CR did not decrease TG content in the fasted state (Fig. 1H).

3.2. Proteome analysis

In WAT, proteome analysis revealed that CR increased the expression of five proteins and reduced the expression of two proteins (Fig. 2 and Table 3). The five proteins up-regulated by CR are involved in metabolic processes. ATP-citrate synthase (ACLY, Spot 1; Berwick et al., 2002; Ramakrishna and Benjamin, 1979), NADP-dependent malic enzyme (MAOX, Spot 2; Taroni and Di Donato, 1988) and long-chain specific acyl-CoA dehydrogenase, mitochondrial (ACADL, Spot 3; Ikeda et al., 1985) are lipid metabolism-related enzymes, and pyruvate dehydrogenase E1 component subunit beta, mitochondrial (ODPB, Spot 4; Huh et al., 1990) and pyruvate carboxylase, mitochondrial (PYC, Spot 5; Jitrapakdee et al., 2006) are glucose metabolism-related enzymes (Table 3). Moreover, three of these five proteins (ACADL, ODPB and PYC) are mitochondrial proteins. In contrast, expression of apolipoprotein A4 (APOA4, Spot 6), which is involved in cholesterol transport (Wang and Paigen, 2005), was attenuated by CR. CR also suppressed the expression of Heat shock protein beta 1 (HSPB1, Spot 7).

In BAT, proteome analysis revealed that CR reduced the expression of four proteins and increased the expression of five proteins (Fig. 3 and Table 4). All four proteins down-regulated by CR [Cytochrome c oxidase subunit 5B (COX5B, Spot 13), NADH dehydrogenase flavoprotein 1, mitochondrial (NAUV1, Spot 14), 2-oxoisovalerate dehydrogenase subunit beta (ODBB, Spot 15) and Succinyl-CoA ligase [ADP-forming] subunit beta, mitochondrial (SUCB1, Spot 16)] are mitochondrial metabolic enzymes. COX5B is one of the small polypeptide subunits composing Complex IV of the mitochondrial electron transport chain, a complex that also contains three large subunits (Capaldi, 1990). NAUV1 is a component of the flavoprotein-sulfur (FP) fragment of Complex I of the mitochondrial electron transport chain (Kerscher et al., 2008). ODBB, also known as branched-chain alpha-keto acid dehydrogenase E1 component alpha chain, catalyzes the reaction from 3-methyl-2-oxobutanoate to 2-methylpropanoyl-CoA, and participates in valine, leucine and isoleucine degradation (She et al., 2007). SUCB1 catalyzes the reaction from succinate to succinyl-CoA in the Krebs cycle (Lambeth et al., 2004). In contrast, Apolipoprotein A1 (APOA1, Spot 8), which is found predominantly in HDL-cholesterols and is involved in cholesterol transport (Wang and Paigen, 2005), was up-regulated by CR. The expression of Tubulin tyrosine ligase-like family, member 10 (TTLL10, Spot 11), which post-translationally modifies tubulin (Ikegami and Setou, 2009) and nucleosome assembly protein 1 (Jahnke et al., 2010), and of Glycerol kinase 5 (GLPK5, Spot 12) were also increased by CR. Interestingly, ACLY (Spot 9) and MAOX (Spot 10) were up-regulated by CR in BAT as well as in WAT. Glycerol kinase, which catalyzes the transfer of a phosphate from ATP to glycerol forming glycerol 3-phosphate, is a primary lipolytic enzyme (Watford, 2000). However, glycerol 3-phosphate is also a substrate for TG formation. Therefore, CR-associated up-regulation of GLPK5 as well as ACLY and MAOX might also activate lipogenesis in BAT (Fig. 3 and Table 4).

Thus, the proteome profile indicates that CR might activate mitochondrial function in WAT, while suppressing the mitochondrial electron transport chain and oxidative phosphorylation in BAT. However, it is likely that CR activates fatty acid biosynthesis similarly in both WAT and BAT.

3.3. Analysis of mitochondrial function

Based on the proteome profile, the relative content of mitochondrial DNA (mtDNA) was measured. The activities of the mitochondrial Krebs cycle enzyme, citrate synthase (CS), and the mitochondrial electron transport chain complex IV (cytochrome c oxidase) were also analyzed (Alp et al., 1976; Dumas et al., 2004; Wiegand and Remington, 1986). In WAT, CR increased the mtDNA content (Fig. 4A) and enhanced CS and complex IV activities in both the fed and fasted states (Fig. 4C). CR reduced the mtDNA content of BAT in the fed state, while fasting increased mtDNA content in CR rats (Fig. 4B). CR did not affect CS activity, but

Please cite this article in press as: Okita, N., et al., Differential responses of white adipose tissue and brown adipose tissue to caloric restriction in rats. Mech. Ageing Dev. (2012), doi:10.1016/j.mad.2012.02.003

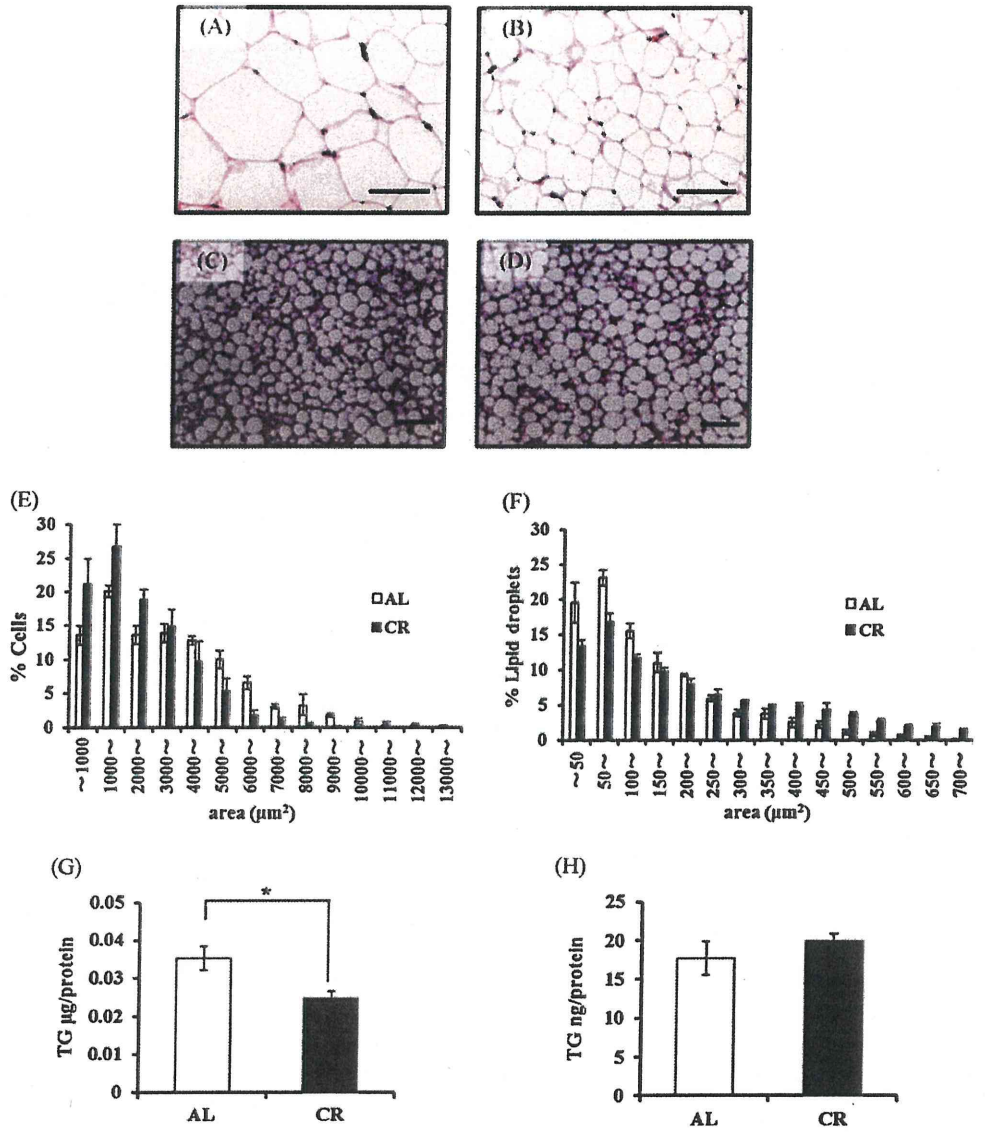

Fig. 1. CR-associated alteration of morphology and triglyceride content in WAT and BAT from AL and CR rats. Representative histological sections of WAT from AL (A) and CR (B) rats (magnification: 40×, scale bar: 100 μm), and of BAT from AL (C) and CR (D) rats (magnification: 200×, scale bar: 50 μm). Sections were stained with hematoxylin–eosin. Based on a quantitative morphometric method using "ImageJ 1.43u/Java1.6.0_22" software, the distribution of adipocyte size in WAT (E) and lipid droplet size in BAT (F) was measured. Triglyceride content of WAT (G) and BAT (H) was also measured. Values shown in all panels are means ± SEM of three to five animals in each group. $^{*}p < 0.05$ by Student's *t*-test.

fasting markedly suppressed it (Fig. 4D). However, Complex IV activity was only slightly reduced by CR (Fig. 4F).

The expression level of several mitochondrial biogenesis-related genes including PGC1α, NRF1, TFAM, COX4 and UCP1 was analyzed by real-time RT-PCR. PGC1α is a transcriptional co-activator that induces mitochondrial biogenesis by activating several transcription factors including NRF1 (Farmer, 2008; Liang and Ward, 2006; Puigserver and Spiegelman, 2003). NRF1 transcriptionally activates TFAM, which drives transcription and replication of the mitochondrial genome as well as transcription of a nuclear-encoded component of Complex IV of the mitochondrial electron transport chain, COX4 (Kang et al., 2007; Lenka et al., 1998; Liang and Ward, 2006; Puigserver and Spiegelman, 2003). The expression of UCP1, which is a BAT-specific protein that contributes to non-shivering thermogenesis, is also transcriptionally regulated *via* the activation of certain nuclear hormone receptors by PGC1α (Liang and Ward, 2006). In WAT, CR up-regulated the expression of PGC1α and COX4 in both fed and fasted states (Fig. 5A and D). CR did not affect the expression of NRF1, but it did increase TFAM levels in the fed state. TFAM expression was also up-regulated by fasting in the AL rats (Fig. 5B and C). In BAT, CR up-regulated the expression of PGC1α in the fed state (Fig. 5F). In contrast, CR down-regulated the expression of COX4, particularly in the fed state (Fig. 5I). CR also down-regulated the expression of both NRF1 and TFAM in the fed state, but not in the fasted state (Fig. 5G and H). Moreover, CR inhibited the expression of UCP1 in both fed and fast states (Fig. 5J).

3.4. Analysis of lipogenesis

As mentioned above, proteome analysis suggested that CR might activate lipogenesis in both WAT and BAT. To confirm these CR-associated changes, we further examined the expression of ACLY (Spot 1 in Fig. 2B and Spot 9 in Fig. 3B). In the 2-DE image of

Please cite this article in press as: Okita, N., et al., Differential responses of white adipose tissue and brown adipose tissue to caloric restriction in rats. Mech. Ageing Dev. (2012), doi:10.1016/j.mad.2012.02.003

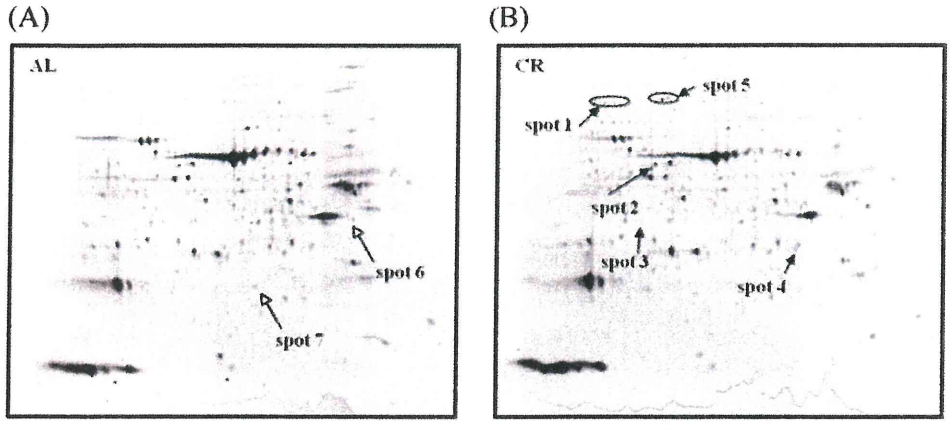

Fig. 2. CR-associated alteration of the protein expression profile of WAT as detected on representative gel images of 2-DE. Protein samples were extracted from WAT of AL-fed and CR-fed rats and separated in pH 3–10 IPG strips for the first dimension and 7.5% SDS–PAGE for the second dimension. Fluorescent gel images stained with SYPRO Ruby were obtained using a FluoroPhoreStar3000 and analyzed with Progenesis PG200 software. Open arrows indicate spots down-regulated by CR, and closed arrows indicate spots up-regulated by CR. 2-DE was performed in duplicate or triplicate for each sample with biological repeats of $n = 3$ for each group.

Table 3

Spot number	Protein description	Function	MW (kDa)	Pi	NCBI accession number (gi)	Mascot score	Sequence coverage (%)	CR fed/AL fed	CR fast/AL fast
1	ATP-citrate synthase (ACLY)	Lipo genesis	121.47	6.96	113116	101	10	>>>	>>>
2	NADP-dependent malic enzyme (MAOX)	Lipo genesis	64.59	6.49	266504	–	–	5.08	3.23
3	Long-chain specific acyl-CoA dehydrogenase, mitochondrial (ACADL)	Mitochondrial beta-oxidation	48.24	7.63	113016	82	18	1.96	1.97
4	Pyruvate dehydrogenase El component subunit beta, mitochondrial (ODPB)	Glycolysis	39.30	6.20	122065728	124	35	>>>	>>>
5	Pyruvate carboxylase, mitochondrial (PYC)	Gluconeogenesis	130.44	6.34	146345499	130	16	3.85	3.17
6	Apolipoprotein A-4 (APOA4)	Cholesterol transport	44.43	5.12	114008	71	13	0.56	0.62
7	Heat shock protein beta-1 (HSPB1)	Stress response	22.94	6.12	1170367	123	30	0.63	0.32

WAT and BAT, CR increased the intensity of Spot 1 and Spot 9, respectively. Moreover, CR increased the number of spots along the X-axis in both Spot 1 and Spot 9, suggesting that CR up-regulated ACLY protein levels and might have altered its post-translational modification in both WAT and BAT. Therefore, the phosphorylated form of ACLY (p-ACLY), which is the active form (Ramakrishna and Benjamin, 1979), and total ACLY (t-ACLY) levels were analyzed. In both WAT and BAT, CR increased p-ACLY and t-ACLY levels in both the fed and fasted states. Increased p-ACLY apparently results from an increased amount of t-ACLY (Fig. 6).

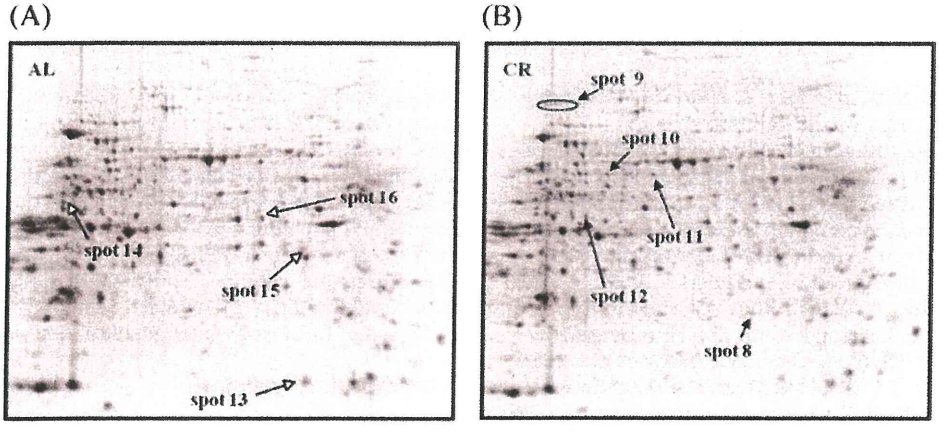

Fig. 3. CR-associated alteration of the protein expression profile of BAT as detected on representative gel images by two-dimensional gel electrophoresis. Protein samples were extracted from BAT of AL-fed and CR-fed rats and separated in pH 3–10 IPG strips for the first dimension and 7.5% SDS–PAGE for the second dimension. Fluorescent gel images stained with SYPRO Ruby were obtained using a FluoroPhoreStar3000 and analyzed with Progenesis PG200 software. Open arrows indicate spots down-regulated by CR, and closed arrows indicate spots up-regulated by CR. 2-DE was performed in duplicate or triplicate for each sample with biological repeats of $n = 3$ for each group.

Please cite this article in press as: Okita, N., et al., Differential responses of white adipose tissue and brown adipose tissue to caloric restriction in rats. Mech. Ageing Dev. (2012), doi:10.1016/j.mad.2012.02.003

Table 4

Spot number	Protein description	Function	MW (kDa)	Pi	NCBI accession number (gi)	Mascot score	Sequence coverage (%)	CR-fed/AL fed	CR-fast/AL fast
8	ApolipoproteinA-1 (APOA1)	Cholesterol transport	30.10	5.52	146345369	80	27	3.77	1.39
9	ATP-citrate synthase (ACLY)	Lipogenesis	121.47	6.96	113116	–	–	2.53	2.27
10	NADP-dependent malic enzyme (MAOX)	Lipogenesis	64.59	6.49	266504	–	–	2.17	3.07
11	Protein polyglycylase TTLL10 (TTL10)	Composition of nicrotuble	78.00	9.55	172045959	52	8	1.93	1.42
12	Putative glycerol kinase 5 (GLPK5)	Lipogenesis	60.34	6.84	172046763	75	14	2.36	1.69
13	Cytochrome c oxidase subunit 5B (COX5B)	Electron transport and oxidative phosphorylation	14.19	7.68	1352167	60	31	0.46	0.64
14	NADH dehydrogenase flavoprotein 1, nitochondrial (NDUV1)	Electron transport and oxidative phosphorylation	51.85	8.51	47117274	82	15	0.60	0.49
15	2-Oxoisovalerate dehydrogenase subunit beta (ODBB)	Branched chain arrrino acid metabolism	43.54	6.41	161784344	54	17	0.57	0.60
16	Succinyl-CoA ligase [ADP-forming] subunit beta, mitochondrial (SUCB1)	Krebs cycle	50.42	6.57	52788305	64	14	0.65	0.49

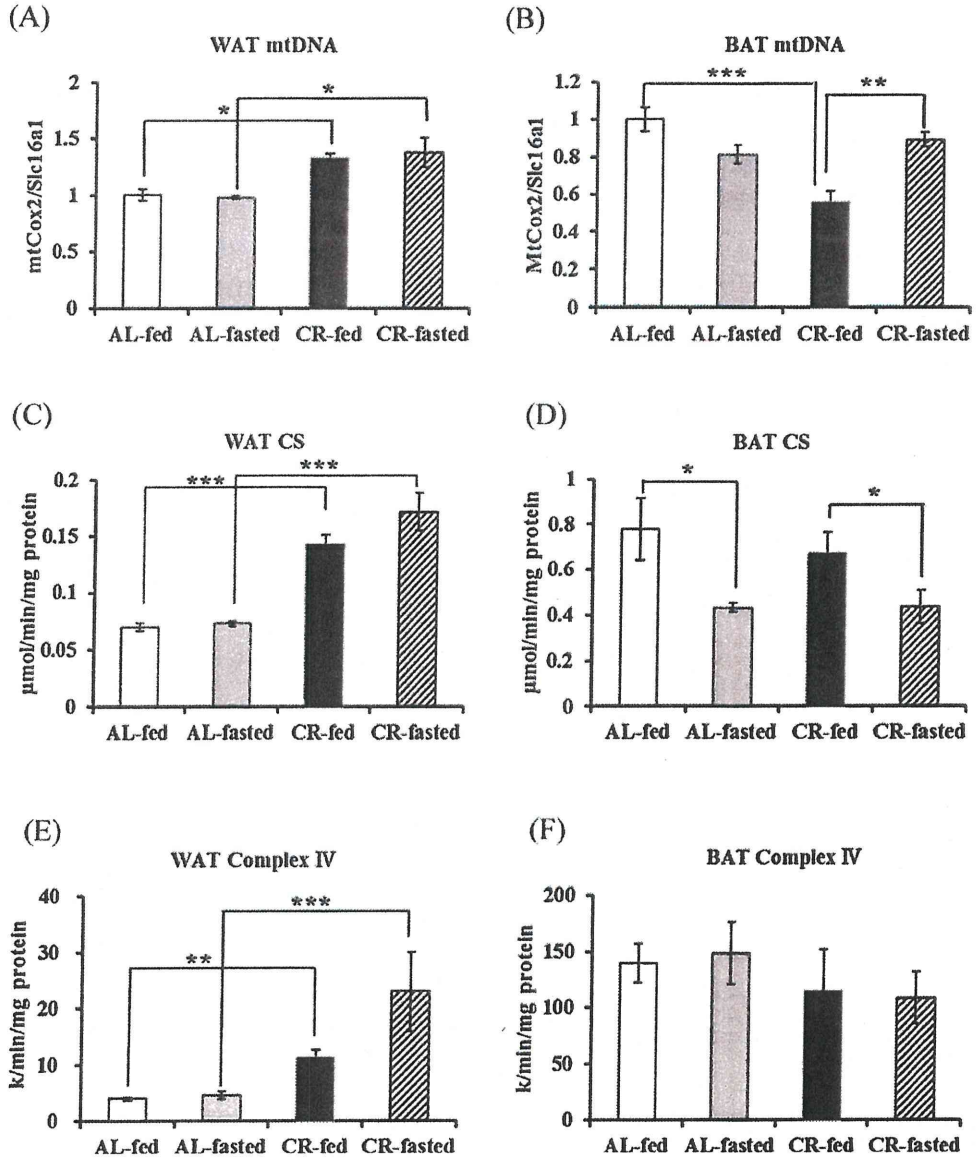

Fig. 4. Effects of CR on mitochondrial DNA content and enzyme activity in WAT and BAT. The ratio of mitochondrial (COX2) *vs.* nuclear (SLC16A1) DNA was obtained by real-time PCR in WAT (A) and BAT (B). Ratios are expressed as the fold change relative to the mean value of AL-fed rats. Citrate synthase activity in WAT (C) and BAT (D) was measured spectrophotometrically at 412 nm. Activity of electron transport chain complex IV and cytochrome c oxidase was measured spectrophotometrically at 550 nm in WAT (E) and BAT (F). Values shown in all panels are means ± SEM of three to five animals in each group. $^{*}p < 0.05$, $^{**}p < 0.01$. $^{***}p < 0.001$ by Tukey's *t*-test.

Please cite this article in press as: Okita, N., et al., Differential responses of white adipose tissue and brown adipose tissue to caloric restriction in rats. Mech. Ageing Dev. (2012), doi:10.1016/j.mad.2012.02.003